

Perturbative QCD analysis of exclusive $J/\psi + \eta_c$ production in e^+e^- annihilation

Ho-Meoyng Choi^a and Chueng-Ryong Ji^b

^a Department of Physics, Teachers College, Kyungpook National University, Daegu, Korea 702-701

^b Department of Physics, North Carolina State University, Raleigh, NC 27695-8202, USA

We analyze the exclusive charmonium $J/\psi + \eta_c$ pair production in e^+e^- annihilation using the nonfactorized perturbative QCD and the light-front quark model(LFQM) that goes beyond the peaking approximation. We effectively include all orders of higher twist terms in the leading order of QCD coupling constant and compare our nonfactorized analysis with the usual factorized analysis in the calculation of the cross section. We also calculate the quark distribution amplitudes, the Gegenbauer moments, and the decay constants for J/ψ and η_c mesons using our LFQM. Our nonfactorized result enhances the NRQCD result by a factor of $3 \sim 4$ at $\sqrt{s} = 10.6$ GeV.

I. INTRODUCTION

It has been known that the exclusive pair production of heavy meson can be reliably predicted within the framework of perturbative quantum chromodynamics(PQCD), since the wave function is well constrained by the nonrelativistic consideration [1]. However, the large discrepancy between the theoretical predictions [2, 3, 4, 5] based on the nonrelativistic QCD(NRQCD) [6] factorization approach and the experimental results [7, 8] for the exclusive $J/\psi + \eta_c$ production in e^+e^- annihilation at the energy $\sqrt{s} = 10.6$ GeV has triggered the need of better understanding both in the available calculational tools and the appreciable relativistic effects.

A particularly convenient and intuitive framework in applying PQCD to exclusive processes is based upon the light-front(LF) Fock-state decomposition of hadronic state. If the PQCD factorization theorem is applicable, then the invariant amplitude for exclusive processes factorizes into the convolution of the valence quark distribution amplitudes(DAs) $\phi(x, q^2)$ with the hard scattering amplitude T_H , which is dominated by one-gluon exchange diagrams at leading order of QCD coupling constant α_s . To implement the factorization theorem at high momentum transfer, the hadronic wave function plays an important role linking between the long distance nonperturbative QCD and the short distance PQCD. In the LF framework, the valence quark DA is computed from the valence LF wave function $\Psi_n(x_i, \mathbf{k}_{\perp i})$ of the hadron at equal LF time $\tau = t + z/c$ which is the probability amplitude to find n constituents(quarks, antiquarks, and gluons) with LF momenta $k_i = (x_i, \mathbf{k}_{\perp i})$ in a hadron. Here, x_i and $\mathbf{k}_{\perp i}$ are the LF longitudinal momentum fraction and the transverse momenta of the i th constituent in the n -particle Fock-state, respectively.

The NRQCD factorization approach [2, 3, 4, 5] for charmonium production assumes that the constituents are sufficiently nonrelativistic so that the relative motion of valence quarks can be neglected inside the meson. In this case, the quark DA becomes the δ function, i.e. $\phi(x, q^2) \sim \delta(x - 1/2)$ (the so-called peaking approximation). However, the cross section value [2, 3, 4, 5] estimated within the NRQCD factorization approach in the leading order of α_s underestimates the experimental

data [7, 8] by an order of magnitude. In order to reduce the discrepancy between theory and experiment, the authors in Refs. [9, 10, 11, 12] considered a rather broad quark DA instead of δ -shaped quark DA.

However, as pointed out in Refs. [13, 14], if the quark DA is not an exact δ function, i.e. \mathbf{k}_{\perp} in the soft bound state LF wave function can play a significant role, the factorization theorem is no longer applicable. To go beyond the peaking approximation, the invariant amplitude should be expressed in terms of the LF wave function $\Psi(x_i, \mathbf{k}_{\perp i})$ rather than the quark DA. In Refs. [13, 14], we discussed the validity issue of peaking approximation for the heavy pseudoscalar meson pair production processes such as $e^+e^- \rightarrow P + P$ ($P = B_c, B_s, B, D, D_s$) using the LF model wave function $\Psi(x_i, \mathbf{k}_{\perp i}) \propto \exp(-M_0^2/\beta^2)$, where M_0 is the invariant mass of the constituent quark and antiquark defined by $M_0^2 = \sum_i(\mathbf{k}_{\perp i}^2 + m_i^2)/x_i$ and β is the gaussian parameter. The gaussian parameter β in our model wave function was found to be related to the transverse momentum via $\beta = \sqrt{\langle \mathbf{k}_{\perp}^2 \rangle}$. This relation naturally explains the zero-binding energy limit as the zero transverse momentum, i.e. $\langle M_0^2 \rangle = (m_1 + m_2)^2$ and $x_i = m_i/M$ for $\beta = 0$. We also found that the heavy quark DA is sensitive to the value of β and indeed quite different from the δ -type DA according to our LFQM based on the variational principle for the QCD-motivated Hamiltonian [15, 16]. In going beyond the peaking approximation, we stressed a consistency of the formulation by keeping the transverse momentum \mathbf{k}_{\perp} both in the wave function part and the hard scattering part together before doing any integration in the amplitude. Similar consideration has also been made in the recent investigation of the relativistic and bound state effects[17] not based on the light-front dynamics(LFD) but including the relativistic effects up to the second order of the relative quark velocity, i.e. $\langle v^2 \rangle$. Such non-factorized analysis should be distinguished from the factorized analysis [9, 10, 11] where the transverse momenta are separately integrated out in the wave function part and in the hard scattering part. Even if the used LF wave functions lead to the similar shapes of DAs, it is apparent that the predictions for the cross sections of heavy meson productions would be different between the factorized and non-factorized analyses.

In this work, we extend our previous works [13, 14] of pseudoscalar meson pair production to the case of pseudoscalar and vector meson productions and calculate the cross section for $e^+e^- \rightarrow J/\psi + \eta_c$ process at leading order of α_s including effectively all orders of higher twist terms. As noted in [14], our results for the quark DA of J/ψ and η_c are quite different from the δ -type function. We find that the non-factorized form of the form factor enhances the cross section of NRQCD result by a factor of $3 \sim 4$ at $\sqrt{s} = 10.6$ GeV while it reduces that of the factorized formulation by 20%. Since the cross section for $e^+e^- \rightarrow J/\psi + \eta_c$ is found to be very sensitive to the behavior of the end points ($x \rightarrow 0$ and 1) in the quark DA, we also examine the results of the decay constants or equivalently the Gegenbauer moments of J/ψ and η_c mesons. Since the perturbative corrections of order α_s to the production amplitude has already been obtained [18] increasing the cross section significantly, it is important to consider the more accurate assessment of cross section at the leading order of α_s .

The paper is organized as follows. In Sec. II, we describe the formulation of our light-front quark model (LFQM), which has been quite successful in describing the static and non-static properties of the pseudoscalar and vector mesons [15, 16]. The formulae for the quark DA, decay constants, Gegenbauer and $\xi(=x_1-x_2)$ moments are also given in this section. In Sec. III, the transverse momentum dependent hard scattering amplitude and the form factor for $e^+e^- \rightarrow J/\psi + \eta_c$ transition are given in leading order of α_s . The form factors both in the factorized and nonfactorized formulations are explicitly given in this section. We also show in this section that our peaking approximation (i.e. NRQCD) result coincides with the one derived from Ma and Si [10]. In Sec. IV, we present the numerical results for the decay constants, quark DAs, Gegenbauer and ξ moments for the J/ψ and η_c mesons and compare them with other theoretical model predictions in addition to the available experimental data. The numerical results for the $e^+e^- \rightarrow J/\psi + \eta_c$ cross section are obtained and compared with the data [7, 8]. Summary and conclusions follow in Sec. V. In the Appendices A and B, we summarize our results for the helicity contributions to the hard scattering amplitudes and the form factor, respectively.

II. MODEL DESCRIPTION

In our LFQM [15, 16], the momentum space light-front wave function of the ground state pseudoscalar and vector mesons is given by

$$\Psi_{100}^{JJ_z}(x_i, \mathbf{k}_{i\perp}, \lambda_i) = \mathcal{R}_{\lambda_1\lambda_2}^{JJ_z}(x_i, \mathbf{k}_{i\perp}) \phi_R(x_i, \mathbf{k}_{i\perp}), \quad (1)$$

where $\phi_R(x_i, \mathbf{k}_{i\perp})$ is the radial wave function and $\mathcal{R}_{\lambda_1\lambda_2}^{JJ_z}$ is the spin-orbit wave function obtained by the interaction independent Melosh transformation from the ordinary equal-time static spin-orbit wave function assigned

by the quantum numbers J^{PC} . The model wave function in Eq. (1) is represented by the Lorentz-invariant variables, $x_i = p_i^+/P^+$, $\mathbf{k}_{i\perp} = \mathbf{p}_{i\perp} - x_i \mathbf{P}_\perp$ and λ_i , where p_i^μ and λ_i are the momenta and the helicities of constituent quarks, respectively, and $P^\mu = (P^+, P^-, \mathbf{P}_\perp) = (P^0 + P^3, (M^2 + \mathbf{P}_\perp^2)/P^+, \mathbf{P}_\perp)$ is the momentum of the meson M .

The covariant forms of the spin-orbit wave functions for pseudoscalar and vector mesons are respectively given by

$$\begin{aligned} \mathcal{R}_{\lambda_1\lambda_2}^{00} &= \frac{-\bar{u}(p_1, \lambda_1) \gamma_5 v(p_2, \lambda_2)}{\sqrt{2}M_0}, \\ \mathcal{R}_{\lambda_1\lambda_2}^{1J_3} &= \frac{-\bar{u}(p_1, \lambda_1) \left[\not{\epsilon}(J_z) - \frac{\epsilon \cdot (p_1 - p_2)}{M_0 + 2m} \right] v(p_2, \lambda_2)}{\sqrt{2}M_0}, \end{aligned} \quad (2)$$

where $\epsilon^\mu(J_z)$ is the polarization vectors of the vector meson, $M_0^2 = (\mathbf{k}_\perp^2 + m^2)/x_1x_2$ is the invariant meson mass square, and $\sum_{\lambda_1\lambda_2} \mathcal{R}_{\lambda_1\lambda_2}^{JJ_z} \mathcal{R}_{\lambda_1\lambda_2}^{JJ_z} = 1$ for both pseudoscalar and vector mesons. Using the four-vectors p_1, p_2 given in terms of the LF relative momentum variables (x, \mathbf{k}_\perp) as

$$\begin{aligned} p_1^+ &= x_1 P^+, \quad p_2^+ = x_2 P^+, \\ \mathbf{p}_{1\perp} &= x_1 \mathbf{P}_\perp + \mathbf{k}_\perp, \quad \mathbf{p}_{2\perp} = x_2 \mathbf{P}_\perp - \mathbf{k}_\perp, \end{aligned} \quad (3)$$

we obtain the explicit forms of spin-orbit wave functions for pseudoscalar and vector mesons with the longitudinal ($\epsilon(0)$) and transverse ($\epsilon(+1)$) polarizations as follows

$$\mathcal{R}_{\lambda_1\lambda_2}^{00} = \frac{1}{C} \begin{pmatrix} -k^L & m \\ -m & -k^R \end{pmatrix}, \quad (4)$$

$$\mathcal{R}_{\lambda_1\lambda_2}^{10} = \frac{1}{C} \begin{pmatrix} k^L \frac{(1-2x)M_0}{M_0+2m} & m + \frac{2\mathbf{k}_\perp^2}{M_0+2m} \\ m + \frac{2\mathbf{k}_\perp^2}{M_0+2m} & -k^R \frac{(1-2x)M_0}{M_0+2m} \end{pmatrix}, \quad (5)$$

$$\mathcal{R}_{\lambda_1\lambda_2}^{11} = \frac{\sqrt{2}}{C} \begin{pmatrix} m + \frac{\mathbf{k}_\perp^2}{M_0+2m} & k^R \frac{x_1 M_0 + m}{M_0+2m} \\ -k^R \frac{x_2 M_0 + m}{M_0+2m} & -\frac{(k^R)^2}{M_0+2m} \end{pmatrix}, \quad (6)$$

where $C = \sqrt{2x_1x_2}M_0$. For the radial wave function ϕ_R , we use the same Gaussian wave function for both pseudoscalar and vector mesons

$$\phi_R(x_i, \mathbf{k}_{i\perp}) = \frac{4\pi^{3/4}}{\beta^{3/2}} \sqrt{\frac{\partial k_z}{\partial x}} \exp(-\vec{k}^2/2\beta^2), \quad (7)$$

where β is the variational parameter. When the longitudinal component k_z is defined by $k_z = (x - 1/2)M_0$, the Jacobian of the variable transformation $\{x, \mathbf{k}_\perp\} \rightarrow k = (\mathbf{k}_\perp, k_z)$ is given by $\partial k_z / \partial x = M_0/(4x_1x_2)$. Also, the normalization factor in Eq. (7) is obtained from the total wave function normalization given by

$$\int_0^1 dx \int \frac{d^2\mathbf{k}_\perp}{16\pi^3} |\Psi_{100}^{JJ_z}(x, \mathbf{k}_\perp, \lambda_1\lambda_2)|^2 = 1. \quad (8)$$

The quark distribution amplitude(DA) of a hadron in our LFQM can be obtained from the hadronic wave function by integrating out the transverse momenta of the quarks in the hadron,

$$\phi(x, \mu) = \int^{\mathbf{k}_\perp^2 < \mu^2} \frac{d^2 \mathbf{k}_\perp}{16\pi^3} \Psi_{100}^{JJ_z}(x, \mathbf{k}_\perp, \lambda_1 \lambda_2), \quad (9)$$

where μ denotes the separation scale between the perturbative and nonperturbative regimes. The dependence on the scale μ is then given by the QCD evolution equation [19] and can be calculated perturbatively. However, the distribution amplitudes at a certain low scale can be obtained by the necessary nonperturbative input from LFQM. The presence of the damping Gaussian factor in our LFQM allows us to perform the integral up to infinity without loss of accuracy. The quark DAs for η_c and J/ψ mesons are constrained by

$$\int_0^1 \phi_{\eta_c(J/\psi)}(x, \mu) dx = \frac{f_{\eta_c(J/\psi)}}{2\sqrt{6}}, \quad (10)$$

where the decay constant is defined as

$$\langle 0 | \bar{q} \gamma^\mu \gamma_5 q | \eta_c \rangle = i f_{\eta_c} P^\mu, \quad (11)$$

for a η_c meson and

$$\begin{aligned} \langle 0 | \bar{q} \gamma^\mu q | J/\psi(P, h) \rangle &= f_{J/\psi} M_{J/\psi} \epsilon^\mu(h), \\ \langle 0 | \bar{q} \sigma^{\mu\nu} q | J/\psi(P, h) \rangle &= i f_{J/\psi}^T [\epsilon^\mu(h) P_\nu - \epsilon^\nu(h) P_\mu], \end{aligned} \quad (12)$$

for a J/ψ meson with longitudinal($h = 0$) and transverse($h = \pm 1$) polarizations, respectively. The constraint of Eq. (10) must be independent of cut-off μ up to corrections of order Λ^2/μ^2 , where Λ is some typical hadronic scale(< 1 GeV) [19]. For the nonperturbative valence wave function given by Eq. (7), we take $\mu \sim m_c$ as an optimal scale for our LFQM description of J/ψ and η_c .

The explicit form of the η_c decay constant is given by [20]

$$\frac{f_{\eta_c}}{2\sqrt{6}} = \int_0^1 dx \int \frac{d^2 \mathbf{k}_\perp}{16\pi^3} \frac{m}{\sqrt{m^2 + \mathbf{k}_\perp^2}} \phi_R(x, \mathbf{k}_\perp). \quad (13)$$

The decay constants for the longitudinally and transversely polarized J/ψ meson are given by [20]

$$\frac{f_{J/\psi}}{2\sqrt{6}} = \int_0^1 dx \int \frac{d^2 \mathbf{k}_\perp}{16\pi^3} \frac{\phi_R(x, \mathbf{k}_\perp)}{\sqrt{m^2 + \mathbf{k}_\perp^2}} \left[m + \frac{2\mathbf{k}_\perp^2}{M_0 + 2m} \right], \quad (14)$$

$$\frac{f_{J/\psi}^T}{2\sqrt{6}} = \int_0^1 dx \int \frac{d^2 \mathbf{k}_\perp}{16\pi^3} \frac{\phi_R(x, \mathbf{k}_\perp)}{\sqrt{m^2 + \mathbf{k}_\perp^2}} \left[m + \frac{\mathbf{k}_\perp^2}{M_0 + 2m} \right], \quad (15)$$

respectively. While the constant $f_{J/\psi}$ is known from the experiment, the constant $f_{J/\psi}^T$ is not that easily accessible in experiment but can be estimated theoretically.

We may also redefine the quark DA as $\Phi_{\eta_c(J/\psi)}(x) = (2\sqrt{6}/f_{\eta_c(J/\psi)})\phi(x)$ for the normalization given by

$$\int_0^1 \Phi_{\eta_c(J/\psi)}(x) dx = 1. \quad (16)$$

The quark DA $\Phi(x)$ evolved in the leading order of $\alpha_s(\mu)$ is usually expanded in Gegenbauer polynomials $C_n^{3/2}$ as

$$\Phi(x, \mu) = \Phi_{\text{as}}(x) \left[1 + \sum_{n=1}^{\infty} a_n(\mu) C_n^{3/2}(2x-1) \right], \quad (17)$$

where $\Phi_{\text{as}}(x) = 6x(1-x)$ is the asymptotic DA and the coefficients $a_n(\mu)$ are Gegenbauer moments [19]. The Gegenbauer moments with $n > 0$ describe how much the DAs deviate from the asymptotic one. In addition to the Gegenbauer moments, we can also define the expectation value of the longitudinal momentum, so-called ξ -moments:

$$\langle \xi^n \rangle = \int_{-1}^1 d\xi \xi^n \hat{\Phi}(\xi) = \int_0^1 dx \xi^n \Phi(x), \quad (18)$$

where $\Phi(x) = 2\hat{\Phi}(2x-1)$ normalized by $\langle \xi^0 \rangle = 1$.

The ξ moments are related to the Gegenbauer moments as follows (up to $n = 6$):

$$\begin{aligned} \langle \xi^2 \rangle &= \frac{1}{5} + a_2 \frac{12}{25}, \\ \langle \xi^4 \rangle &= \frac{3}{35} + a_2 \frac{8}{35} + a_4 \frac{8}{77}, \\ \langle \xi^6 \rangle &= \frac{1}{21} + a_2 \frac{12}{77} + a_4 \frac{120}{1001} + a_6 \frac{64}{2145}. \end{aligned} \quad (19)$$

III. HARD CONTRIBUTIONS TO $e^+e^- \rightarrow J/\psi + \eta_c$ PROCESS

For the exclusive process

$$e^+e^- \rightarrow \gamma^*(q) \rightarrow J/\psi(P_V) + \eta_c(P_P), \quad (20)$$

the form factor is defined as

$$\langle J/\psi(P_V, h) \eta_c(P_P) | J_{\text{em}}^\mu | 0 \rangle = \epsilon^{\mu\nu\rho\sigma} \epsilon_\nu^* P_{V\rho} P_{P\sigma} \mathcal{F}(q^2), \quad (21)$$

where $\epsilon_\nu^*(P_V, h)$ is the polarization vector of the vector meson with four momentum P_V and helicity h . The cross section can be calculated as

$$\sigma(e^+e^- \rightarrow J/\psi \eta_c) = \frac{\pi\alpha^2}{6} |\mathcal{F}(s)|^2 \left(1 - \frac{4M_h^2}{s} \right)^{3/2}, \quad (22)$$

where we neglect the small mass difference between J/ψ and η_c , i.e. $M_h \approx M_{J/\psi} \approx M_{\eta_c}$.

At leading order of α_s , the contribution to the form factor comes from four Feynman diagrams; one of them is shown in Fig. 1. To obtain the timelike form factor $\mathcal{F}(q^2)$ for the process $e^+e^- \rightarrow \gamma^* \rightarrow J/\psi \eta_c$, we first calculate

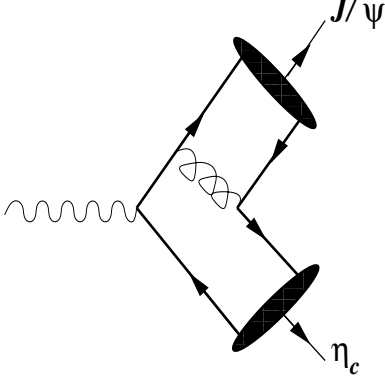


FIG. 1: One of the four Feynman diagrams for the amplitude.

the radiative decay process $\eta_c(P) + \gamma^*(q) \rightarrow J/\psi(P')$ using the Drell-Yan-West ($q^+ = q^0 + q^3 = 0$) frame

$$P = \left(P^+, \frac{M_{\eta_c}^2}{P^+}, \mathbf{0}_\perp \right), P' = \left(P^+, \frac{M_{J/\psi}^2 + \mathbf{q}_\perp^2}{P^+}, \mathbf{q}_\perp \right),$$

$$q = \left(0, \frac{\mathbf{q}_\perp^2}{P^+}, \mathbf{q}_\perp \right), \quad (23)$$

where the four momentum transfer is spacelike, i.e. $q^2 = q^+q^- - \mathbf{q}_\perp^2 = -\mathbf{q}_\perp^2 < 0$. We then analytically continue the spacelike form factor $\mathcal{F}(\mathbf{q}_\perp^2)$ to the timelike $q^2 > 0$ region by changing $-\mathbf{q}_\perp^2$ to q^2 in the form factor.

In the calculations of the form factor $\mathcal{F}(q^2)$, we use the ‘+’-component of currents and the transverse ($h = \pm 1$) polarization for J/ψ given by

$$\epsilon^*(\pm 1) = \mp \frac{1}{\sqrt{2}} \left(0, \frac{2q^L}{P^+}, 1, \mp i \right), \quad (24)$$

where $q^L = q_x - iq_y$. For the longitudinal ($h = 0$) polarization, it is hard to extract the form factor since both sides of Eq. (21) vanish for any q^2 value. In the energy region where PQCD is applicable, the hadronic matrix element $\langle J/\psi | J_{\text{em}}^+ | \eta_c \rangle$ can be calculated within the leading order PQCD by means of a homogeneous Bethe-Salpeter (BS) equation for the meson wave function. Formally, one may consider a contribution even at lower order without any gluon exchange as often called Feynman mechanism. However, we don’t need to take this contribution into account in this work because we are considering the production process of heavy mesons that ought to require high momentum transfer between the primary quark-antiquark pair production and the secondary quark-antiquark pair production in order to get the final state heavy mesons. Since the final bound state wavefunctions satisfy the BS type iterative bound state equation, one gluon exchange can be generated by iteration from the wavefunction part even if the scattering amplitude formally has no gluon exchange. We thus generate the hard gluon exchange from the iteration of bound state wavefunction and consider the leading order

PQCD contribution in the framework of LFD. The secondary quark-antiquark pair production can occur only through the gluon momentum transfer due to the rational light-front energy-momentum dispersion relation. The quark-antiquark pair production from the vacuum is suppressed in the LFD and the absence of zero-mode contribution can be shown by the direct power counting method that we presented in our previous work of weak transition form factors between pseudoscalar and vector mesons [21]. Taking the perturbative kernel of the BS equation as a part of hard scattering amplitude T_H , one thus obtains

$$\begin{aligned} \langle J/\psi | J_{\text{em}}^+ | \eta_c \rangle &= \sum_{\lambda, \lambda'} \int [d^3k] [d^3l] \Psi_{100}^{11\dagger}(y, \mathbf{l}_\perp, \lambda) \\ &\times T_H(x, \mathbf{k}_\perp; y, \mathbf{l}_\perp; \mathbf{q}_\perp; \lambda, \lambda') \\ &\times \Psi_{100}^{00}(x, \mathbf{k}_\perp, \lambda'), \end{aligned} \quad (25)$$

where $[d^3k] = dx d^2\mathbf{k}_\perp / 16\pi^3$ and T_H contains all two-particle irreducible amplitudes for $\gamma^* + q\bar{q} \rightarrow q\bar{q}$ from the iteration of the LFQM wave function with the BS kernel. On the other hand, the right-hand-side of Eq. (21) for the matrix element of J^+ is obtained as

$$\langle J/\psi | J_{\text{em}}^+ | \eta_c \rangle = \frac{P^+}{\sqrt{2}} q^L \mathcal{F}(q^2). \quad (26)$$

Here, we set $P^+ = 1$ without any loss of generality. Therefore, we get the form factor as

$$\mathcal{F}(q^2) = \int [d^3k] [d^3l] \phi_R(y, \mathbf{l}_\perp) \mathcal{T}_H \phi_R(x, \mathbf{k}_\perp), \quad (27)$$

where we combined the spin-orbit wave function into the original T_H to form a new \mathcal{T}_H , i.e.

$$\begin{aligned} \mathcal{T}_H &= \frac{\sqrt{2}}{q^L} \sum_{\lambda, \lambda'} \mathcal{R}_{\lambda'_1 \lambda'_2}^{11\dagger}(y, \mathbf{l}_\perp) T_H(x, \mathbf{k}_\perp; y, \mathbf{l}_\perp; \mathbf{q}_\perp; \lambda, \lambda') \\ &\times \mathcal{R}_{\lambda_1 \lambda_2}^{00}(x, \mathbf{k}_\perp). \end{aligned} \quad (28)$$

We should note that the form factor $\mathcal{F}(q^2)$ has a dimension $[1/\text{GeV}]$ so that the cross section has a dimension of [barn] where $1 \text{ GeV}^{-2} = 0.39 \text{ mb}$ in the natural unit ($\hbar = c = 1$). Since the measure $[d^3k]$ has the dimension of $[\text{GeV}^2]$ and our radial wave function ϕ_R has the dimension of $[1/\text{GeV}]$, the amplitude \mathcal{T}_H has the dimension of $[1/\text{GeV}^3]$.

The leading order light-front time-ordered diagrams for the meson form factor are shown in Fig. 2, where the

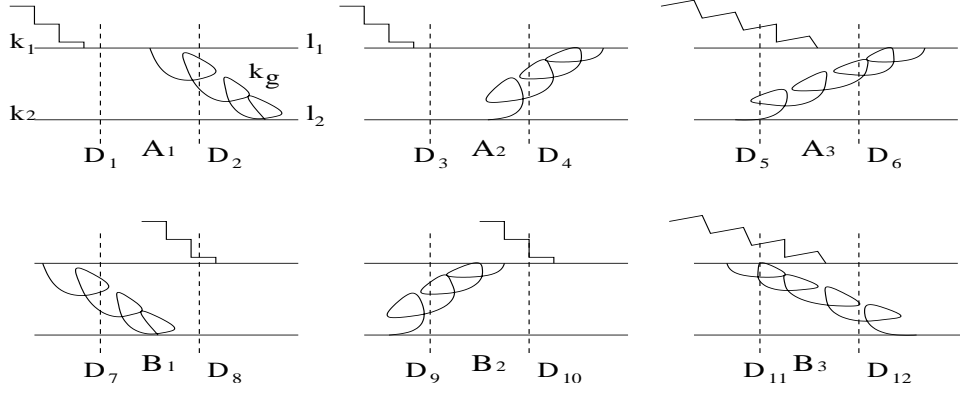


FIG. 2: Leading order(in α_s) light-front time-ordered diagrams of the hard scattering amplitude for $\eta_c(P) \rightarrow \gamma^*(q) + J/\psi(P')$ process.

energy denominators are given by

$$\begin{aligned}
D_1 &= M^2 + \mathbf{q}_\perp^2 - \frac{(\mathbf{k}_\perp + \mathbf{q}_\perp)^2 + m^2}{x_1} - \frac{\mathbf{k}_\perp^2 + m^2}{x_2}, \\
D_2 &= M^2 + \mathbf{q}_\perp^2 - \frac{(y_1 \mathbf{q}_\perp + \mathbf{l}_\perp)^2 + m^2}{y_1} - \frac{\mathbf{k}_\perp^2 + m^2}{x_2} \\
&\quad - \frac{(y_2 \mathbf{q}_\perp + \mathbf{k}_\perp - \mathbf{l}_\perp)^2}{y_2 - x_2}, \\
D_3 &= D_1, \\
D_4 &= M^2 + \mathbf{q}_\perp^2 - \frac{(\mathbf{k}_\perp + \mathbf{q}_\perp)^2 + m^2}{x_1} \\
&\quad - \frac{(y_2 \mathbf{q}_\perp + \mathbf{k}_\perp - \mathbf{l}_\perp)^2}{x_2 - y_2} - \frac{(y_2 \mathbf{q}_\perp - \mathbf{l}_\perp)^2 + m^2}{y_2}, \\
D_5 &= M^2 - \frac{\mathbf{k}_\perp^2 + m^2}{x_1} - \frac{(y_2 \mathbf{q}_\perp + \mathbf{k}_\perp - \mathbf{l}_\perp)^2}{x_2 - y_2} \\
&\quad - \frac{(y_2 \mathbf{q}_\perp - \mathbf{l}_\perp)^2 + m^2}{y_2}, \\
D_6 &= D_4, \\
D_7 &= M^2 - \frac{(\mathbf{l}_\perp - y_2 \mathbf{q}_\perp)^2 + m^2}{y_1} - \frac{\mathbf{k}_\perp^2 + m^2}{x_2} \\
&\quad - \frac{(y_2 \mathbf{q}_\perp + \mathbf{k}_\perp - \mathbf{l}_\perp)^2}{y_2 - x_2}, \\
D_8 &= M^2 - \frac{(\mathbf{l}_\perp - y_2 \mathbf{q}_\perp)^2 + m^2}{y_1} - \frac{(\mathbf{l}_\perp - y_2 \mathbf{q}_\perp)^2 + m^2}{y_2}, \\
D_9 &= D_5, D_{10} = D_8, D_{11} = D_7, D_{12} = D_2. \tag{29}
\end{aligned}$$

According to the rules of light-front perturbation theory, the hard scattering amplitude for the diagram A_1 in Fig. 2 is given by

$$\begin{aligned}
T_{A_1} &= (-1) \frac{\theta(k_g^+)}{k_g^+ D_1 D_2} \bar{u}(k_1 + q) \gamma^+ u(k_1) \\
&\quad \times \left[4\pi\alpha_s C_F \bar{u}(l_1) \gamma^\mu u(k_1 + q) d_{\mu\nu}^{(k_g)} \bar{v}(k_2) \gamma^\nu v(l_2) \right] \\
&= (-2)(4\pi\alpha_s C_F) \frac{\theta(k_g^+)}{k_g^+ D_1 D_2} N_{A_1} \tag{30}
\end{aligned}$$

where $N_{A_1} = \bar{u}(l_1) \gamma^\mu u(k_1 + q) d_{\mu\nu}^{(k_g)} \bar{v}(k_2) \gamma^\nu v(l_2)$ is the gluon-fermion vertex part with the gauge dependent polarization sum $d_{\mu\nu}$ for the gluon, $C_F = 4/3$ is the color factor and the notation $u(p)$ denotes actually $u(p)/\sqrt{p^+}$ for the internal fermions in a scattering amplitude. In the Feynman gauge, the polarization sum $d^{\mu\nu}$ equals to $g^{\mu\nu}$. In the light-front gauge $\eta \cdot A = A^+ = 0$,

$$\begin{aligned}
d_{\mu\nu}^{(k_g)} &= \sum_{\lambda=1,2} \epsilon_\mu(k_g, \lambda) \epsilon_\nu(k_g, \lambda) \\
&= -g_{\mu\nu} + \frac{\eta_\mu(k_g) \nu + \eta_\nu(k_g) \mu}{k_g^+}, \tag{31}
\end{aligned}$$

where $k_g \cdot \epsilon = \eta \cdot \epsilon = 0$. Since the gluon propagator has an instantaneous part $(\eta^\mu \eta^\nu / (k_g^+)^2)$ in the light-front gauge, we absorb this instantaneous contribution into the regular propagator by replacing k_g by $\bar{k}_g = (y_2 - x_2, \bar{k}_g^-, y_2 \mathbf{q}_\perp + \mathbf{k}_\perp - \mathbf{l}_\perp)$, where $\bar{k}_g^- = P^- + q^- - l_1^- - k_2^-$ includes the instantaneous contribution.

Similarly, the hard scattering amplitude for the diagram A_2 in Fig. 2 is given by

$$T_{A_2} = (-2)(4\pi\alpha_s C_F) \frac{\theta(k_g^+)}{k_g^+ D_3 D_4} N_{A_2}, \tag{32}$$

where N_{A_2} has the same form as N_{A_1} but with different gluon momentum $\bar{k}_g = (x_2 - y_2, \bar{k}_g^-, \mathbf{l}_\perp - y_2 \mathbf{q}_\perp - \mathbf{k}_\perp)$. The diagram A_2 has also the instantaneous contribution and absorb it into $\bar{k}_g^- = P^- + q^- - (k_1 + q)^- - l_2^-$. The hard scattering amplitude for the diagram A_3 in Fig. 2 is given by

$$T_{A_3} = (-2)(4\pi\alpha_s C_F) \frac{\theta(k_g^+)}{k_g^+ D_5 D_6} N_{A_3}, \tag{33}$$

where N_{A_3} has also the same form as N_{A_1} or N_{A_2} . However, in this case we have just regular gluon propagator with the four momentum $k_g = (x_2 - y_2, k_g^-, \mathbf{l}_\perp - y_2 \mathbf{q}_\perp - \mathbf{k}_\perp)$ and $k_g^+ = \mathbf{k}_{g\perp}^2 / k_g^+$ since the diagram does not have the instantaneous part.

Likewise, one can obtain the hard scattering amplitudes corresponding to the diagrams B_i .

If one includes the higher twist effects such as intrinsic transverse momenta and the quark masses, the LF gauge part proportional to $1/k_g^+$ leads to a singularity although the Feynman gauge part $g_{\mu\nu}$ gives the regular amplitude. This is due to the gauge-invariant structure of the amplitudes. The covariant derivative $D_\mu = \partial_\mu + igA_\mu$ makes both the intrinsic transverse momenta, \mathbf{k}_\perp and \mathbf{l}_\perp , and the transverse gauge degree of freedom $g\mathbf{A}_\perp$ be of the same order, indicating the need of the higher Fock state contributions to ensure the gauge invariance [22]. However, we can show that the sum of six diagrams for the LF gauge part ($1/k_g^+$ terms) vanishes in the limit that the LF energy differences Δ_x and Δ_y go to zero, where Δ_x and Δ_y are given by

$$\begin{aligned}\Delta_x &= M^2 - \frac{\mathbf{k}_\perp^2 + m^2}{x_1 x_2} = M^2 - M_{0x}^2, \\ \Delta_y &= M^2 - \frac{\mathbf{l}_\perp^2 + m^2}{y_1 y_2} = M^2 - M_{0y}^2.\end{aligned}\quad (34)$$

Details of the proof can be found in our previous work [14]. In this work, we follow the same procedure presented in Ref. [14] and calculate the higher twist effects in the limit of $\Delta_x = \Delta_y = 0$ to avoid the involvement of the higher Fock state contributions. Our limit $\Delta_x = \Delta_y = 0$ (but $\sqrt{\langle \mathbf{k}_\perp^2 \rangle} = \beta \neq 0$) may be considered as a zeroth order approximation in the expansion of a scattering amplitude. That is, the scattering amplitude T_H may be expanded in terms of LF energy difference Δ as $T_H = [T_H]^{(0)} + \Delta[T_H]^{(1)} + \Delta^2[T_H]^{(2)} + \dots$, where $[T_H]^{(0)}$ corresponds to the amplitude in the zeroth order of Δ . This approximation should be distinguished from

the zero-binding(or peaking) approximation that corresponds to $M = m_1 + m_2$ and $\mathbf{k}_\perp = \beta = 0$. The point of this distinction is to note that $[T_H]^{(0)}$ includes the binding energy effect(i.e. $\mathbf{k}_\perp, \mathbf{l}_\perp \neq 0$) that was neglected in the peaking approximation.

In zeroth order of Δ , one can show that the energy denominators entering in the diagrams A_i and B_i ($i = 1, 2, 3$) have the following relations

$$\mathcal{D}_2 + \mathcal{D}_4 = \mathcal{D}_1, \mathcal{D}_2 + \mathcal{D}_5 = 0, \mathcal{D}_2 + \mathcal{D}_8 = \mathcal{D}_7, \quad (35)$$

where $\mathcal{D}_i = \lim_{\Delta_x = \Delta_y = 0} D_i$ and

$$\begin{aligned}\mathcal{D}_1 &= -(x_2 \mathbf{q}_\perp^2 + 2\mathbf{k}_\perp \cdot \mathbf{q}_\perp)/x_1, \\ \mathcal{D}_8 &= -(y_2 \mathbf{q}_\perp^2 - 2\mathbf{l}_\perp \cdot \mathbf{q}_\perp)/y_1, \\ \mathcal{D}_2 &= -[x_2^2 y_2^2 \mathbf{q}_\perp^2 + x_2^2 \mathbf{l}_\perp^2 + y_2^2 \mathbf{k}_\perp^2 - 2x_2 y_2 (x_2 \mathbf{l}_\perp \cdot \mathbf{q}_\perp \\ &\quad - y_2 \mathbf{k}_\perp \cdot \mathbf{q}_\perp + \mathbf{k}_\perp \cdot \mathbf{l}_\perp) + (y_2 - x_2)^2 m^2] \\ &\quad / [x_2 y_2 (y_2 - x_2)].\end{aligned}\quad (36)$$

As one can see from Eqs. (4) and (6), the leading twist(LT)(i.e. neglecting transverse momenta \mathbf{k}_\perp and \mathbf{l}_\perp) helicity contributions for $\eta_c(P) + \gamma^*(q) \rightarrow J/\psi(P', \epsilon(+1))$ process come from two leading helicity $\Delta H = |\lambda_{J/\psi} - \lambda_{\eta_c}| = 1$ components, i.e. $\uparrow\downarrow \rightarrow \uparrow\uparrow$ and $\downarrow\uparrow \rightarrow \uparrow\uparrow$ as in the nonrelativistic spin case, i.e. $\frac{1}{\sqrt{2}}(|\uparrow\downarrow\rangle - |\downarrow\uparrow\rangle)$ for η_c meson to $|\uparrow\uparrow\rangle$ for J/ψ meson.

In Table I, we summarize our results for the hard scattering amplitude T_H for these two leading helicity $\Delta H = 1$ components in zeroth order of binding energy limit. For instance, $\sum_{i=1}^3 T_{A_i}^{(\uparrow\downarrow \rightarrow \uparrow\uparrow)}$ and $\sum_{i=1}^3 T_{B_i}^{(\uparrow\downarrow \rightarrow \uparrow\uparrow)}$ are obtained as

$$\begin{aligned}\left[\sum_i T_{A_i}^{(\uparrow\downarrow \rightarrow \uparrow\uparrow)}\right]_{\Delta=0} &= -8\pi\alpha_s C_F N_{A_1}^{(\uparrow\downarrow \rightarrow \uparrow\uparrow)} \left[\frac{\theta(y_2 - x_2)}{(y_2 - x_2)\mathcal{D}_1\mathcal{D}_2} + \frac{\theta(x_2 - y_2)}{(x_2 - y_2)} \left(\frac{1}{\mathcal{D}_3\mathcal{D}_4} + \frac{1}{\mathcal{D}_5\mathcal{D}_6} \right) \right] \\ &= -8\pi\alpha_s C_F N_{A_1}^{(\uparrow\downarrow \rightarrow \uparrow\uparrow)} \left[\frac{1}{(y_2 - x_2)\mathcal{D}_1\mathcal{D}_2} \right], \\ \left[\sum_i T_{B_i}^{(\uparrow\downarrow \rightarrow \uparrow\uparrow)}\right]_{\Delta=0} &= -8\pi\alpha_s C_F N_{B_1}^{(\uparrow\downarrow \rightarrow \uparrow\uparrow)} \left[\frac{\theta(y_2 - x_2)}{(y_2 - x_2)} \left(\frac{1}{\mathcal{D}_7\mathcal{D}_8} + \frac{1}{\mathcal{D}_{11}\mathcal{D}_{12}} \right) + \frac{\theta(x_2 - y_2)}{(x_2 - y_2)\mathcal{D}_9\mathcal{D}_{10}} \right] \\ &= -8\pi\alpha_s C_F N_{B_1}^{(\uparrow\downarrow \rightarrow \uparrow\uparrow)} \left[\frac{1}{(y_2 - x_2)\mathcal{D}_2\mathcal{D}_8} \right].\end{aligned}\quad (37)$$

To derive the final results in Eq. (37), we use the following identities obtained from Eqs. (29) and (35):

$$\begin{aligned}\frac{1}{\mathcal{D}_3\mathcal{D}_4} + \frac{1}{\mathcal{D}_5\mathcal{D}_6} &= \frac{1}{\mathcal{D}_1\mathcal{D}_4} + \frac{1}{\mathcal{D}_5\mathcal{D}_4} \\ &= \frac{\mathcal{D}_1 + \mathcal{D}_5}{\mathcal{D}_1\mathcal{D}_4\mathcal{D}_5} = \frac{\mathcal{D}_1 - \mathcal{D}_2}{\mathcal{D}_1\mathcal{D}_4(-\mathcal{D}_2)} \\ &= \frac{-1}{\mathcal{D}_1\mathcal{D}_2},\end{aligned}\quad (38)$$

for the diagram A and

$$\begin{aligned}\frac{1}{\mathcal{D}_7\mathcal{D}_8} + \frac{1}{\mathcal{D}_{11}\mathcal{D}_{12}} &= \frac{1}{\mathcal{D}_7\mathcal{D}_8} + \frac{1}{\mathcal{D}_7\mathcal{D}_2} \\ &= \frac{\mathcal{D}_2 + \mathcal{D}_8}{\mathcal{D}_7\mathcal{D}_2\mathcal{D}_8} = \frac{1}{\mathcal{D}_2\mathcal{D}_8}, \\ \frac{1}{\mathcal{D}_9\mathcal{D}_{10}} &= \frac{1}{\mathcal{D}_5\mathcal{D}_8} = \frac{-1}{\mathcal{D}_2\mathcal{D}_8},\end{aligned}\quad (39)$$

for the diagram B. The above identities lead to $\theta(y_2 -$

TABLE I: Leading helicity contributions to the hard scattering amplitudes, $T_H^{(\uparrow\downarrow\rightarrow\uparrow\uparrow)}$ and $T_H^{(\downarrow\uparrow\rightarrow\uparrow\uparrow)}$. The momentum variable $p^{R(L)}$ represents $p^{R(L)} = p_x \pm ip_y$.

$ \Delta H = 1 $	$N_{A_1} = N_{A_2} = N_{A_3}$	$\sum_{i=1}^3 T_{A_i}(\Delta_x = \Delta_y = 0)$	$N_{B_1} = N_{B_2} = N_{B_3}$	$\sum_{i=1}^3 T_{B_i}(\Delta_x = \Delta_y = 0)$
$\uparrow\downarrow\rightarrow\uparrow\uparrow$	$\frac{2m(x_1 l - y_1 k - x_2 y_1 q)^L}{x_2 y_1 y_2}$	$-\frac{8\pi\alpha_s C_F}{(y_2 - x_2)\mathcal{D}_1 \mathcal{D}_2} N_{A_1}^{(\uparrow\downarrow\rightarrow\uparrow\uparrow)}$	$\frac{2m(x_1 l - y_1 k - x_1 y_2 q)^L}{x_2 y_1 y_2}$	$-\frac{8\pi\alpha_s C_F}{(y_2 - x_2)\mathcal{D}_2 \mathcal{D}_8} N_{B_1}^{(\uparrow\downarrow\rightarrow\uparrow\uparrow)}$
$\downarrow\uparrow\rightarrow\uparrow\uparrow$	$-\frac{2m(x_2 l - y_2 k - x_2 y_2 q)^L}{x_1 y_1 y_2}$	$-\frac{8\pi\alpha_s C_F}{(y_2 - x_2)\mathcal{D}_1 \mathcal{D}_2} N_{A_1}^{(\downarrow\uparrow\rightarrow\uparrow\uparrow)}$	$-\frac{2m(x_2 l - y_2 k - x_2 y_2 q)^L}{x_1 y_1 y_2}$	$-\frac{8\pi\alpha_s C_F}{(y_2 - x_2)\mathcal{D}_2 \mathcal{D}_8} N_{B_1}^{(\downarrow\uparrow\rightarrow\uparrow\uparrow)}$

$x_2) + \theta(x_2 - y_2) = 1$ in Eq. (37).

By adding all six LF time-ordered diagrams, we obtain

$$[T_H^{(\uparrow\downarrow\rightarrow\uparrow\uparrow)}]^{(0)} = \sum_{i=1}^3 \left[T_{A_i}^{(\uparrow\downarrow\rightarrow\uparrow\uparrow)} + T_{B_i}^{(\uparrow\downarrow\rightarrow\uparrow\uparrow)} \right]_{\Delta=0}. \quad (40)$$

Similarly, one can easily obtain the helicity $\downarrow\uparrow\rightarrow\uparrow\uparrow$ contribution to the hard scattering amplitude, $T_H^{(\downarrow\uparrow\rightarrow\uparrow\uparrow)}$ from Table I.

In the numerical calculations for the higher twist contributions, one may keep effectively only the leading order of higher twist terms such as $\mathbf{k}_\perp^2/\mathbf{q}_\perp^2$, $\mathbf{l}_\perp^2/\mathbf{q}_\perp^2$, and $\mathbf{k}_\perp \cdot \mathbf{l}_\perp/\mathbf{q}_\perp^2$ due to the fact that $\mathbf{k}_\perp^2 \ll \mathbf{q}_\perp^2$ and $\mathbf{l}_\perp^2 \ll \mathbf{q}_\perp^2$ in large momentum transfer region where PQCD is applicable [14, 23]. As shown in our previous work [14], this can be done by neglecting the subleading higher twist terms accordingly both in the energy denominators and the numerators for the hard scattering amplitude T_H . This procedure is very similar to the recent investigation of the relativistic and bound state effects not based on the LFD but including the relativistic effects up to the second order of the relative quark velocity, i.e. $\langle v^2 \rangle$ [17]. Indeed, our numerical result neglecting the higher orders of $\mathbf{k}_\perp^2/\mathbf{q}_\perp^2$, $\mathbf{l}_\perp^2/\mathbf{q}_\perp^2$ and $\mathbf{k}_\perp \cdot \mathbf{l}_\perp/\mathbf{q}_\perp^2$ is very close to that presented in Ref.[17] (see Section IV). However, in this work, we include all higher orders of $\mathbf{k}_\perp^2/\mathbf{q}_\perp^2$, $\mathbf{l}_\perp^2/\mathbf{q}_\perp^2$ and $\mathbf{k}_\perp \cdot \mathbf{l}_\perp/\mathbf{q}_\perp^2$. This corresponds to keep effectively all higher orders of the relative quark velocity beyond $\langle v^2 \rangle$. We compare our full result with the one neglecting the corrections of order $\mathcal{O}(\langle v^4 \rangle)$.

Using Eq. (28), we then obtain the leading helicity contributions to the hard scattering amplitude combined with the spin-orbit wave function in zeroth order of Δ as follows

$$\begin{aligned} [\mathcal{T}_H]^{(0)} &= \frac{\sqrt{2}}{q^L} \mathcal{R}_{\uparrow\uparrow}^{11\dagger} \left[T_H^{(\uparrow\downarrow\rightarrow\uparrow\uparrow)} \mathcal{R}_{\uparrow\uparrow}^{00} + T_H^{(\downarrow\uparrow\rightarrow\uparrow\uparrow)} \mathcal{R}_{\uparrow\uparrow}^{00} \right] \\ &= \frac{m}{\sqrt{m^2 + \mathbf{k}_\perp^2}} \frac{\left[m + \frac{\mathbf{l}_\perp^2}{M_{0y} + 2m} \right]}{\sqrt{m^2 + \mathbf{l}_\perp^2}} \mathcal{M}_H, \end{aligned} \quad (41)$$

where

$$\begin{aligned} \mathcal{M}_H &= \frac{16\pi\alpha_s C_F m}{x_1 x_2 y_1 y_2 (y_2 - x_2) q^2} \left[(x_1^2 + x_2^2) l^L q^R \right. \\ &\quad \left. - (x_1 y_1 + x_2 y_2) k^L q^R \right] \left(\frac{1}{\mathcal{D}_1 \mathcal{D}_2} + \frac{1}{\mathcal{D}_2 \mathcal{D}_8} \right) \\ &\quad + \frac{16\pi\alpha_s C_F m}{x_1 x_2 y_1 y_2 (y_2 - x_2)} \left[\frac{x_2 (x_1 y_1 + x_2 y_2)}{\mathcal{D}_1 \mathcal{D}_2} \right. \\ &\quad \left. + \frac{y_2 (x_1^2 + x_2^2)}{\mathcal{D}_2 \mathcal{D}_8} \right], \end{aligned} \quad (42)$$

and $l^L q^R = \mathbf{l}_\perp \cdot \mathbf{q}_\perp + i|\mathbf{l}_\perp \times \mathbf{q}_\perp|$. Accordingly, the leading helicity contributions to the form factor lead to the following non-factorized form

$$\begin{aligned} \mathcal{F}(q^2) &= Q_c \int [d^3 k] [d^3 l] \phi_R(x, \mathbf{k}_\perp) [\mathcal{T}_H]^{(0)} \phi_R(y, \mathbf{l}_\perp) \\ &\quad + Q_c (m_1 \leftrightarrow m_2), \\ &= 2Q_c \int [d^3 k] [d^3 l] \frac{m}{\sqrt{m^2 + \mathbf{k}_\perp^2}} \phi_R(x, \mathbf{k}_\perp) \mathcal{M}_H \\ &\quad \times \frac{1}{\sqrt{m^2 + \mathbf{l}_\perp^2}} \left[m + \frac{\mathbf{l}_\perp^2}{M_{0y} + 2m} \right] \phi_R(y, \mathbf{l}_\perp), \end{aligned} \quad (43)$$

where $Q_c = 2/3$ is the charge fraction of charm quark in the unit of e .

In the leading twist(LT) limit neglecting the transverse momenta, the hard scattering amplitude in Eq. (42) is reduced to

$$\mathcal{M}_H^{\text{LT}} = \frac{16\pi\alpha_s C_F m}{x_1 x_2 y_1 y_2^2 q^4} [x_1 (x_1 y_1 + x_2 y_2) + y_1 (x_1^2 + x_2^2)]. \quad (44)$$

Then, the form factor in Eq. (43) factorizes into the convolution of the nonperturbative valence quark DAs $\phi_{\eta_c(J/\psi)}(x, \mu)$ with the perturbative hard scattering amplitude $\mathcal{M}_H^{\text{LT}}$:

$$\begin{aligned} \mathcal{F}^{\text{LT}}(q^2) &= 2Q_c \int_0^1 dx \int_0^1 dy \phi_{\eta_c}(x, \mu) \\ &\quad \times \mathcal{M}_H^{\text{LT}}(x_i, y_i, q^2) \phi_{J/\psi}^T(y, \mu), \end{aligned} \quad (45)$$

where $\phi_{J/\psi}^T(y, \mu)$ is the quark DA for the transversely polarized J/ψ meson. Furthermore, in nonrelativistic QCD(NRQCD) limit(i.e. peaking approximation) where the longitudinal momentum fractions are given by $x_i =$

$y_i \approx 1/2$ with $M_h \approx 2m_c$, the quark DAs for both η_c and J/ψ mesons become δ -type functions, i.e.

$$\phi_{\eta_c(J/\psi)}^\delta(x, \mu) = \frac{f_{\eta_c(J/\psi)}}{2\sqrt{6}}\delta(x - 1/2), \quad (46)$$

and the form factor in NRQCD limit is reduced to

$$\mathcal{F}^\delta(q^2) \approx 2Q_c \frac{f_{\eta_c} f_{J/\psi}}{(2\sqrt{6})^2} \frac{256\pi\alpha_s(\mu)C_F}{q^4} M_h, \quad (47)$$

where the superscript δ for the quark DA in Eq. (46) and the form factor in Eq. (47) represents the NRQCD result. Our NRQCD result [40] is exactly the same as that derived from Ma and Si in Ref. [10](see Eqs. (16) and (21) in [10]).

Other subleading helicity contributions to the hard scattering amplitude that show up as next-to-leading order in transverse momenta are summarized in Tables IV and V of the Appendix A.

IV. NUMERICAL RESULTS

In our numerical calculations, we use our LFQM [15, 16] parameters (m_c, β_{cc}) obtained from the meson spectroscopy with the variational principle for the QCD motivated effective Hamiltonian. In our LFQM, we have used the two interaction potentials $V_{Q\bar{Q}}$ for η_c and J/ψ mesons: (1) Coulomb plus harmonic oscillator(HO) potential, and (2) Coulomb plus linear confining potential. In addition, the hyperfine interaction essential for the distinction between J/ψ and η_c mesons is included for both cases (1) and (2), viz.,

$$V_{Q\bar{Q}} = a + V_{\text{conf}} - \frac{4\alpha_s}{3r} + \frac{32\pi}{9} \frac{\alpha_s}{m_c^2} \vec{S}_Q \cdot \vec{S}_{\bar{Q}} \delta^3(\vec{r}), \quad (48)$$

where $V_{\text{conf}} = br^2$ for the HO potential and br for the linear confining potential, respectively. For the linear confining potential, we use the string tension $b = 0.18 \text{ GeV}^2$, which is rather well known from other quark-model analysis commensurate with the Regge phenomenology [24]. The other potential model parameters are then fixed by the variational principle for the central Hamiltonian with respect to the Gaussian parameter β . For instance, the model parameters for the linear confining potential are obtained as $a = -0.724 \text{ GeV}$, $m_c = 1.8 \text{ GeV}$, and the strong coupling constant $\alpha_s(\mu) = 0.313$ defined by

$$\alpha_s(\mu) = \frac{12\pi}{(33 - 2N_f)\ln(\mu^2/\Lambda^2)}, \quad (49)$$

where $N_f = 4$ is the number of active flavors(u, d, s and c). At scale $\mu \simeq m_c$ for charmonium, our value of $\Lambda = 162 \text{ MeV}$, the scale associated with nonperturbative effects involving light quarks and gluons, is consistent with the usual $\Lambda_{QCD} \simeq 200 \text{ MeV}$. Our value of $\alpha_s = 0.313$ is also quite comparable with other quark model predictions

TABLE II: Decay constants[MeV] of η_c and J/ψ obtained from our variational parameters ($m_c = 1.8, \beta$)[GeV] and compared with the experimental data.

	Linear ($\beta = 0.6509$)	HO ($\beta = 0.6998$)	HO' ($\beta = 0.7278$)	Exp.
f_{η_c}	326	354	370	335 ± 75 [29]
$f_{J/\psi}$	360	395	416	416 ± 6 [30]
$f_{J/\psi}^T$	343	375	393	—

such as 0.35, 0.45, $0.30 \sim 0.38$, and 0.314 from ISGW2 model [25], Cornell potential model [26], Bodwin-Kang-Lee(BKL) model [27](in next-to-leading order in α_s), and relativistic quark model [17], respectively. Lattice measurements of the heavy-quark potential yield the values for effective coupling α_s of 0.22 in the quenched case and approximately 0.26 in the unquenched case [28]. The HO potential model parameters are obtained in a similar way as in the case of the linear potential. We should note that the root-mean-square value of the transverse momentum in our LFQM is equal to the Gaussian β value, i.e. $\sqrt{\langle \mathbf{k}_\perp^2 \rangle_{cc}} = \beta_{cc}$.

In Table II, we summarize our results for decay constants of η_c and J/ψ obtained from our variational parameters ($m_c = 1.8 \text{ GeV}$, $\beta_{cc} = 0.6509 \text{ GeV}$) for the linear potential[second column] and ($m_c = 1.8 \text{ GeV}$, $\beta_{cc} = 0.6998 \text{ GeV}$) for the HO potential[third column]. Our results for the decay constants $f_{\eta_c} = 326$ [354] MeV, $f_{J/\psi} = 360$ [395] MeV, and $f_{J/\psi}^T = 343$ [375] MeV obtained from the linear[HO] potential parameters are quite comparable with the current experimental data, $(f_{\eta_c})_{\text{exp}} = 335 \pm 75 \text{ MeV}$ [29] and $(f_{J/\psi})_{\text{exp}} = 416 \pm 6 \text{ MeV}$ [30] as well as other theoretical model calculations such as the QCD sum rules [31, 32] in which the decay constants were obtained as $f_{\eta_c} = 346 \text{ MeV}$, $f_{J/\psi} = 412 \text{ MeV}$ and $f_{J/\psi}^T = 409 \text{ MeV}$. As a sensitivity check of our variational parameters, we include in Table II another Gaussian parameters($m_c = 1.8 \text{ GeV}$, $\beta_{cc} = 0.7278 \text{ GeV}$) to fit the central value of the experimental J/ψ decay constant. We denote this as HO' in Table II. In the following numerical calculations, we present all of these three cases (linear, HO, HO') to show the parameter sensitivity of our results.

The shape of the quark DA which depends on (m_c, β_{cc}) values is important to the calculation of the cross section for the heavy meson pair production in e^+e^- annihilations. We thus show in Fig. 3 the normalized quark DA for η_c and J/ψ , $\phi_{c\bar{c}}(x) = \phi_{\eta_c}(x) \approx \phi_{J/\psi}(x)$ obtained from linear(dotted line), HO(solid line), and HO'(dashed line) potentials compared with the ones obtained from Bondar and Chernyak(BC) [9] (dot-dashed line) and from QCD sum rules [31](doubledot-dashed line). As one can see from Fig. 3, our quark DA $\phi_{c\bar{c}}(x)$ obtained at scale $\mu \simeq m_c$ practically vanishes in the regions $x < 0.1$ and $x > 0.9$ where the motion of $c\bar{c}$ pair is expected to be highly relativistic. However, our results for quark DA are certainly wider than the delta function-type(i.e. $\beta_{cc} \rightarrow 0$

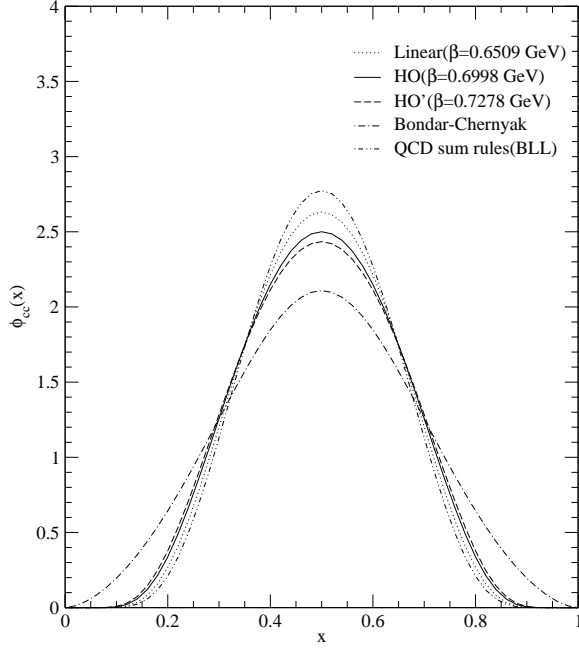


FIG. 3: The leading twist distribution amplitudes $\phi(x)$ for η_c and J/ψ [$\phi_{\eta_c}(x) \approx \phi_{J/\psi}(x)$] obtained from our LFQM compared with the ones from Bondar-Chernyak model [9] and QCD sum rules [31].

limit) NRQCD results [2, 3, 4], which do not take into account the relative motion of valence quark-antiquark pair. Our results also show that the shape of quark DA becomes broader and more enhanced at the endpoint region ($x \rightarrow 0$ or 1) as the Gaussian parameter β (or equivalently transverse \mathbf{k}_\perp -size) increases. In comparison with other theoretical model calculations, we find that our result is quite consistent with the one obtained from QCD sum rules [31] at scale $\mu \simeq m_c$ but much narrower than the one obtained from BC [9]. As will be discussed later, the cross section for double-charm production is indeed very sensitive to the end point behavior of the quark DA.

In Table III, we list the calculated $\langle \xi^n \rangle$ moments up to $n = 6$ for the η_c and J/ψ DAs at scale $\mu \simeq m_c$ and compare with other model estimates. Our central, upper and lower values are obtained from HO, HO' and linear parameters, respectively. Since the ξ moments for J/ψ meson with the longitudinal polarization are almost the same as those with the transverse polarization, our results imply that $\langle \xi^n \rangle_{J/\psi} = \langle \xi^n \rangle_L = \langle \xi^n \rangle_T$, which is also confirmed by the recent QCD sum rule calculations [31, 32]. Furthermore, the ξ moments between η_c and J/ψ mesons are not much different from each other as one can see from Table III. Our results for the ξ moments are in good agreement with those obtained from other potential models [26, 33] as well as QCD sum-rules [31, 32], but disagree with the predictions obtained from BC [9] and BKL [27] models. While NRQCD predictions [34] for the second and fourth moments are in agreement with our model but disagree for the higher moment $\langle \xi^6 \rangle$. This

disagreement for the moment $\langle \xi^6 \rangle$ may be ascribed to the end point behavior (i.e. relativistic correction) of quark DA.

Within our model calculation, the relative quark velocity can be obtained from the relation $m_r v^2/2 \simeq 2\sqrt{m_c^2 + \vec{k}^2} - 2m_c$ in the center of mass frame, where m_r is the reduced mass. From this relation, we obtain $v^2 \simeq 2\mathbf{k}_\perp^2/m_c^2 = 2\beta^2/m_c^2$, i.e.

$$\langle v^2 \rangle_{c\bar{c}} = 0.30_{-0.04}^{+0.02}, \quad (50)$$

where the central, upper, and lower values are from the HO, HO', and linear potential parameters, respectively. Using the dimensional regularization at leading order of α_s , the authors in Refs. [31, 32] derived the relation between the relative velocity of quark-antiquark pair inside the charmonium and the ξ moment as $\langle \xi^n \rangle_{\eta_c} \approx \langle \xi^n \rangle_{J/\psi} = \langle v^n \rangle / (n+1)(n=2, 4, 6)$. Applying this formula to our model calculations, we get the relative v^2 as $\langle v^2 \rangle_{c\bar{c}} = 0.25_{-0.02}^{+0.01}$, where again the central, upper, and lower values are from the HO, HO', and linear potential parameters, respectively. The results obtained from our LFQM and QCD sum rule methods are not only in an agreement with each other but also quite consistent with the value $\langle v^2 \rangle_{c\bar{c}} \approx 0.3$ used in NRQCD [2, 27]. Note that one gets the quark DA $\phi(x) \sim \delta(x - 1/2)$ in the limit $v \rightarrow 0$ while $\phi(x) \sim \phi_{as}(x) = 6x(1-x)$ as $v \rightarrow 1$. As noted in QCD sum rule calculations [31], the moments $\langle \xi^n \rangle$ are proportional to v^n according to the NRQCD v -scaling rules [6]: $(m_c v^2)^2 \ll (m_c v)^2 \ll m_c^2$. It is not difficult to see that the ξ -moments obtained from our LFQM and QCD sum rules [31] satisfy these rules. However, as discussed in [31], the BC moments [9] break the NRQCD v -scaling rules and the quark DA obtained from [9] corresponds to the QCD sum rule result [31] defined at scale $\mu \simeq 10$ GeV rather than at $\mu \simeq m_c$. In our LFQM calculation, we would overestimate the experimental values of decay constants for J/ψ and η_c if we were to use the shape of BC distribution to get the cross section value of double-charm production consistent with the experimental data. Thus, it seems misleading to claim that the cross section of $e^+e^- \rightarrow J/\psi + \eta_c$ in [9] led to a good agreement with the experiment.

The corresponding Gegenbauer moments obtained from Eq. (19) are given by

$$\begin{aligned} a_2(\mu \simeq m_c) &= -0.339_{-0.021}^{+0.011}, \\ a_4(\mu \simeq m_c) &= 0.082_{+0.022}^{-0.010}, \\ a_6(\mu \simeq m_c) &= +0.0027_{-0.0112}^{+0.0041}, \end{aligned} \quad (51)$$

for η_c meson and

$$\begin{aligned} a_2(\mu \simeq m_c) &= -0.343_{-0.020}^{+0.011}, \\ a_4(\mu \simeq m_c) &= 0.087_{+0.020}^{-0.010}, \\ a_6(\mu \simeq m_c) &= -0.0015_{-0.0067}^{+0.0035}, \end{aligned} \quad (52)$$

for J/ψ meson, respectively. Since a_n for J/ψ with longitudinal polarization and a_n^T with transverse polarization

TABLE III: The ξ moments $\langle \xi^n \rangle_{\eta_c}$ and $\langle \xi^n \rangle_{J/\psi} = \langle \xi^n \rangle_L \approx \langle \xi^n \rangle_T$ for η_c and J/ψ distribution amplitudes obtained from our LFQM at the scale $\mu \simeq m_c$ and compared with other model($\langle \xi^n \rangle_{\eta_c} \approx \langle \xi^n \rangle_{J/\psi}$) estimates. Our central, upper, and lower values are obtained from the HO, HO', and linear potential parameters, respectively.

$\langle \xi^n \rangle$	Ours $\langle \xi^n \rangle_{\eta_c}$	Ours $\langle \xi^n \rangle_{J/\psi}$	Buchmuller Tye model [33]	Cornell model [26]	BC [9]	BKL [27]	NRQCD [34]	QCD sum rules [31, 32]
$n = 2$	$0.084^{+0.004}_{-0.007}$	$0.082^{+0.004}_{-0.006}$	0.086	0.084	0.13	0.019	0.075 ± 0.011	0.070 ± 0.007
$n = 4$	$0.017^{+0.003}_{-0.003}$	$0.016^{+0.002}_{-0.002}$	0.020	0.019	0.040	0.0083	0.010 ± 0.003	0.012 ± 0.002
$n = 6$	$0.0047^{+0.0006}_{-0.0010}$	$0.0046^{+0.0005}_{-0.0010}$	0.0066	0.0066	0.018	0.0026	0.0017 ± 0.0007	0.0031 ± 0.0008

are not much different from each other, we do not distinguish them in our model calculation.

In Fig. 4, we show $s^2 \mathcal{F}(s)$ for $e^+e^- \rightarrow J/\psi + \eta_c$ process. The left panel of Fig. 4 shows the results obtained from the central value $\beta = 0.6998$ GeV of our model parameters displaying different (leading and subleading) helicity contributions. The right panel of Fig. 4 shows the sensitivity of our model predictions with all helicity contributions when the gaussian model parameter β changes as shown in Fig. 3. In the left panel, the dotted and short-dashed lines represent the results obtained from the non-relativistic peaking approximation $\mathcal{F}^\delta(s)$ [Eq. (47)] and the leading twist (LT) factorized form factor $\mathcal{F}^{\text{LT}}(s)$ [Eq. (45)] taking into account the relative motion of valence quarks, respectively. The long-dashed line represents the higher twist (HT) nonfactorized form factor $\mathcal{F}^{\text{HT}}(s)$ [Eq. (43)] obtained by including the transverse momenta ($\mathbf{k}_\perp, \mathbf{l}_\perp$) both in the wave function and the hard scattering part. Note that $\mathcal{F}^\delta(s)$ (dotted line), $\mathcal{F}^{\text{LT}}(s)$ (short-dashed line), and $\mathcal{F}^{\text{HT}}(s)$ (long-dashed line) are obtained from the leading helicity contributions. The solid line represents our full solution $\mathcal{F}_{(\Delta H=0+\Delta H=1)}^{\text{HT}}(s)$ including all (leading plus subleading) helicity contributions summarized in the Appendix A (Tables IV and V). Among the subleading helicity contributions, we find that only $\uparrow\uparrow \rightarrow \uparrow\uparrow$ (dot-dashed line) and $(\uparrow\downarrow \rightarrow \uparrow\downarrow) + (\downarrow\uparrow \rightarrow \downarrow\uparrow)$ (double-dot-dashed line) helicity contributions give a sizeable effects and other subleading helicity contributions are negligible. As shown in Fig. 4, we find that while $s^2 \mathcal{F}_{(\Delta H=0+\Delta H=1)}^{\text{HT}}(s)$ is about 2 times larger than $s^2 \mathcal{F}^\delta(s)$ but 10% smaller than $s^2 \mathcal{F}^{\text{LT}}(s)$ at $\sqrt{s} = 10.6$ GeV. It is also interesting to note that our $s^2 \mathcal{F}_{(\Delta H=0+\Delta H=1)}^{\text{HT}}(s)$ takes over $s^2 \mathcal{F}^{\text{LT}}(s)$ for $\sqrt{s} \gtrsim 13$ GeV region, although $s^2 \mathcal{F}^{\text{HT}}(s)$ with leading helicity components approaches to $s^2 \mathcal{F}^{\text{LT}}(s)$ as $s \rightarrow \infty$. As one can see from Fig. 4, the form factor obtained from our calculation shows $\mathcal{F}(s) \sim s^{-2}$ as $s \rightarrow \infty$ which is the expected QCD scaling behavior [10, 35, 36, 37, 38, 39] for the transition form factor between pseudoscalar (0^{-+}) and vector (1^{--}) mesons.

In Fig. 5, we show leading order in α_s contribution to the cross section for $e^+e^- \rightarrow J/\psi + \eta_c$. The left panel of Fig. 5 shows the results with leading and subleading helicity contributions using the HO model parameters. The right panel of Fig. 5 shows the sensitivity of our model predictions with all helicity contributions when the gaussian model parameter β changes as shown in Figs. 3 and

4. The line codes are the same as in Fig. 4. As one can see from the left panel of Fig. 5, our peaking approximation result (dotted line) is consistent with the previous NRQCD estimates in Refs. [2, 3, 4], which is an order of magnitude smaller than the experimental data [7, 8]. We should note from the left panel of Fig. 5 that our higher twist result (solid line) including all helicity contributions enhances the peaking approximation result by a factor of $3 \sim 4$ at $\sqrt{s} = 10.6$ GeV while it reduces that of the leading twist result by 20%. As discussed in Section III, our higher twist results (σ_{HT}) include all orders of $\mathbf{k}_\perp^2/\mathbf{q}_\perp^2$, $\mathbf{l}_\perp^2/\mathbf{q}_\perp^2$ and $\mathbf{k}_\perp \cdot \mathbf{l}_\perp/\mathbf{q}_\perp^2$ to keep effectively all higher orders of the relative quark velocity beyond $\langle v^2 \rangle$. If we keep only the leading order of these terms ($\mathbf{k}_\perp^2/\mathbf{q}_\perp^2$, $\mathbf{l}_\perp^2/\mathbf{q}_\perp^2$ and $\mathbf{k}_\perp \cdot \mathbf{l}_\perp/\mathbf{q}_\perp^2$), our results would correspond to include the relativistic effects up to the order of $\langle v^2 \rangle$ [17]. Our predictions for the cross section at $\sqrt{s} = 10.6$ GeV obtained from peaking approximation (σ_δ), leading twist (σ_{LT}) and higher twist (σ_{HT}) are given by

$$\begin{aligned}\sigma_\delta(J/\psi + \eta_c) &= 2.34^{+0.50}_{-0.69} [\text{fb}], \\ \sigma_{\text{LT}}(J/\psi + \eta_c) &= 10.57^{+3.15}_{-4.02} [\text{fb}], \\ \sigma_{\text{HT}}^{(\Delta H=0+\Delta H=1)}(J/\psi + \eta_c) &= 8.76^{+1.61}_{-2.84} [\text{fb}],\end{aligned}\quad (53)$$

where the central, upper and lower values are obtained from HO, HO' and linear potential parameters, respectively. Our prediction of $\sigma_{\text{HT}}^{(\Delta H=0+\Delta H=1)}(J/\psi + \eta_c)$ reduces by about 10% from the value in Eq. (53) to $7.68^{+1.94}_{-2.66} [\text{fb}]$ when we keep only the leading order of $\mathbf{k}_\perp^2/\mathbf{q}_\perp^2$, $\mathbf{l}_\perp^2/\mathbf{q}_\perp^2$ and $\mathbf{k}_\perp \cdot \mathbf{l}_\perp/\mathbf{q}_\perp^2$. It is interesting to note that our reduced value $7.68^{+1.94}_{-2.66} [\text{fb}]$ is indeed very close to the result 7.8 [fb] obtained in the recent investigation including the relativistic effects up to $\langle v^2 \rangle$ [17].

As a sensitivity check, we show in Fig. 6 the parameter (m_c, β) dependence of the cross section for $e^+e^- \rightarrow J/\psi + \eta_c$ using the nonfactorized higher twist form factor with all helicity contributions. We also show in Fig. 6 the decay constants corresponding to the end point mass values, $m_c = 1.4$ GeV and 1.8 GeV. The cross section increases as $\beta(m_c)$ increases (decreases). As one can also see from Fig. 6, the cross section is more sensitive to the variation of the gaussian parameter than to the variation of the charm quark mass.

The experimental results are

$$\sigma(J/\psi + \eta_c) \times B^{\eta_c}[\geq 2] = (25.6 \pm 2.8 \pm 3.4) [\text{fb}], \quad (54)$$

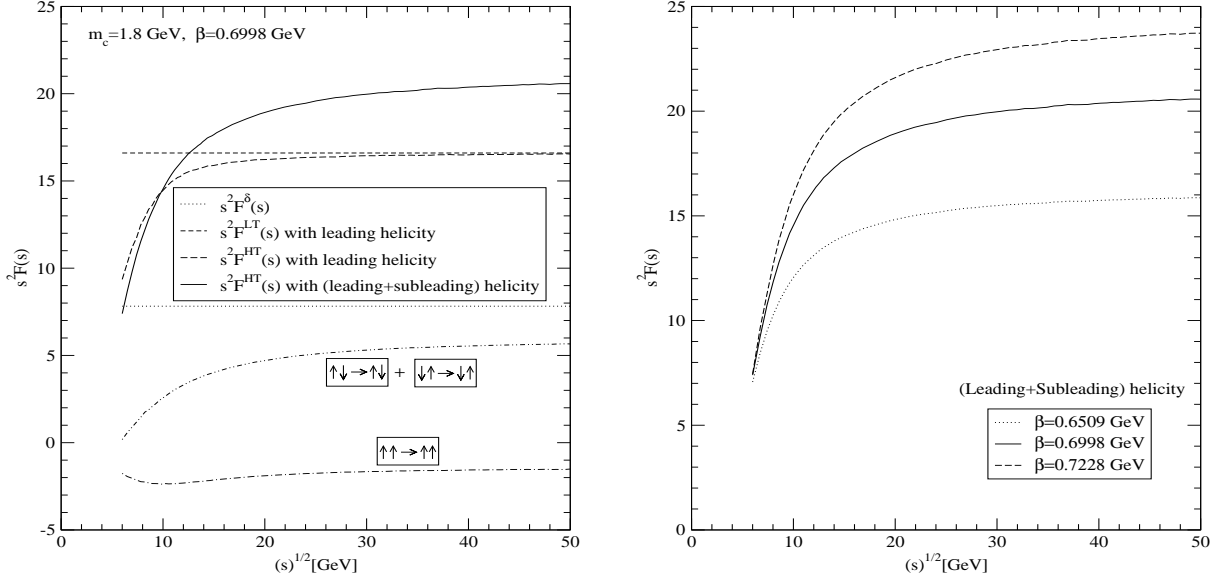


FIG. 4: The form factor $s^2 \mathcal{F}(s)$ for $e^+e^- \rightarrow J/\psi + \eta_c$. The dotted, short-dashed, long-dashed and solid line in left panel represent the peaking, leading twist(LT), higher twist(HT) results with the leading helicity contributions and HT one with all helicity contributions, respectively. The dot-dashed and double-dot-dashed line represent the dominant subleading contributions. The right panel represents the HT results including all helicity contributions obtained from linear(dotted line), HO(solid line), and HO'(dashed line) model parameters, respectively.

by Belle [7](filled circle in Fig 5) and

$$\sigma(J/\psi + \eta_c) \times B^{\eta_c}[\geq 2] = (17.6 \pm 2.8_{-2.1}^{+1.5})[\text{fb}], \quad (55)$$

by Babar [8](filled square in Fig 5), where $B^{\eta_c}[\geq 2]$ is the branching fraction for η_c decay into at least two charged particles. Considering an enhancement by the factor of 1.8 from the corrections of next-to-leading order (NLO) of α_s [18], it might be conceivable to raise our leading α_s order result $\sigma_{\text{HT}}^{(\Delta H=0+\Delta H=1)}(J/\psi + \eta_c)$ in Eq.(53) by this factor and get a value close to the above Babar data. However, it would be necessary to make detailed NLO investigation within the LF PQCD framework before we can make any firm conclusion.

V. SUMMARY AND CONCLUSION

We investigated the transverse momentum effect on the exclusive charmonium $J/\psi + \eta_c$ pair production in e^+e^- annihilation using the nonfactorized PQCD and LFQM that goes beyond the peaking approximation.

Our LFQM calculation based on the variational principle for the QCD-motivated Hamiltonian [15, 16] shows that the quark DAs for J/ψ and η_c take substantially broad shape which is quite different from the δ -type DA. If the quark DA is not an exact δ function, i.e. the relative motion of valence quarks can play a significant role, the factorization theorem is no longer applicable.

In going beyond the peaking approximation, we stressed a consistency by keeping the transverse momentum \mathbf{k}_\perp both in the wave function part and the hard scattering part simultaneously before doing any integration in the amplitude. Such non-factorized analysis should be distinguished from the factorized analysis where the transverse momenta are separately integrated out in the wave function part and in the hard scattering part. Even if the used LF wave functions lead to the similar shapes of DAs, predictions for the cross sections of double-charm productions are apparently different between the factorized and non-factorized analyses. We found that the higher twist contributions including all helicity contributions enhanced NRQCD result by a factor of $3 \sim 4$ at $\sqrt{s} = 10.6 \text{ GeV}$ while it reduced that of the leading twist result by 20%. We also found that the cross section for $e^+e^- \rightarrow J/\psi \eta_c$ process at $\sqrt{s} = 10.6 \text{ GeV}$ is more sensitive to the variation of the gaussian parameter than to that of the charm quark mass. Our results showed that the cross section increases as $\beta(m_c)$ increases(decreases).

In conclusion, LFQM/PQCD analysis showed that the relativistic correction(i.e. non-delta function) of the light-front wave function is very important to understand the large discrepancy between the NRQCD result and the experimental data given by Eqs.(54) and (55). While there have been considerations of broadening the quark DA to reduce the discrepancy between the theory at the leading order of α_s and the experimental results[9, 10, 11], a recent calculation of corrections of

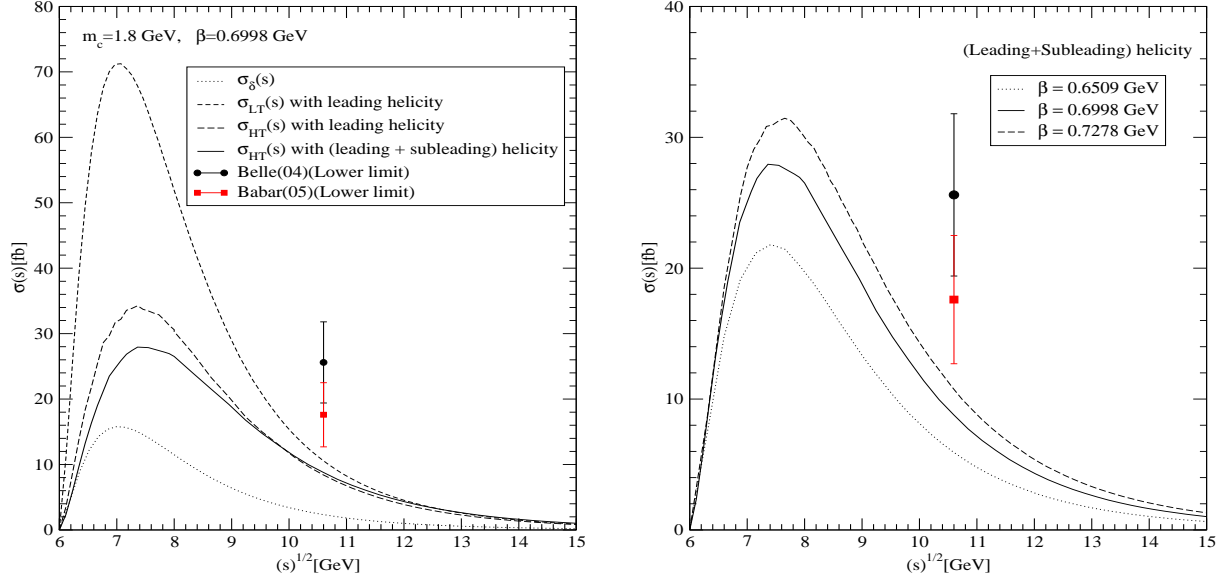


FIG. 5: The cross section for $e^+e^- \rightarrow J/\psi\eta_c$ with leading and subleading helicity contributions using the HO model parameters(left panel) and with all helicity contributions using the linear, HO, and HO' model parameters(right panel).

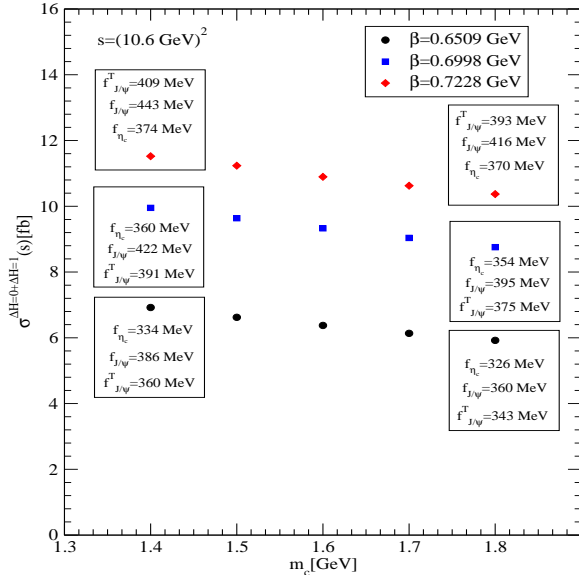


FIG. 6: The parameter (m_c, β) dependence of the cross section for $e^+e^- \rightarrow J/\psi + \eta_c$.

next-to-leading order(NLO) of α_s leads to an enhance-

ment of the theoretical prediction by the factor about 1.8 [18]. This factor may enhance our result in the leading order of α_s to fit the current experimental results. However, more detailed investigation is necessary prior to any firm conclusion on this issue.

Acknowledgments

This work was supported by a grant from the U.S. Department of Energy(No. DE-FG02-03ER41260). H.-M. Choi was supported in part by Korea Research Foundation under the contract KRF-2005-070-C00039. The National Energy Research Scientific Center is also acknowledged for the grant of supercomputing time.

APPENDIX A: HELICITY CONTRIBUTIONS TO THE HARD SCATTERING AMPLITUDE

In this appendix A, we summarize the helicity contributions $(\lambda_1, \lambda_2) \rightarrow (\lambda'_1, \lambda'_2)$ to the hard scattering amplitude $T_H^{(\lambda_1, \lambda_2) \rightarrow (\lambda'_1, \lambda'_2)}$ for the $\eta_c(P) \rightarrow \gamma^*(q) + J/\psi(P')$ process.

In Tables IV and V, we summarize our results for the helicity contributions to the hard scattering amplitudes T_A and T_B for the diagrams in Fig. 2, where

$$\begin{aligned}
P_{A1} &= \frac{-2}{x_1 x_2 y_1 y_2} \left[x_2^2 y_1 y_2 \mathbf{q}_\perp^2 + x_1 x_2 \mathbf{l}_\perp^2 + y_1 y_2 \mathbf{k}_\perp^2 + x_2(x_1 y_1 + x_2 y_2)(\mathbf{l}_\perp \cdot \mathbf{q}_\perp) \right. \\
&\quad \left. + 2x_2 y_1 y_2(\mathbf{k}_\perp \cdot \mathbf{q}_\perp) + (x_1 y_1 + x_2 y_2)(m^2 + \mathbf{k}_\perp \cdot \mathbf{l}_\perp) \right] + \frac{2}{(x_1 - y_1)}[D_2 + D_4] = P_A + \frac{2}{(x_1 - y_1)}[D_2 + D_4], \\
P_{A2} &= P_A + \frac{2}{(x_1 - y_1)}[D_2 + D_4], \quad P_{A3} = P_A + \frac{2}{(x_1 - y_1)}[D_2 - D_4], \\
Q_A &= \frac{2}{x_1 x_2 y_1 y_2} \left[x_2(x_1 - y_2)|\mathbf{l}_\perp \times \mathbf{q}_\perp| - 2x_1 y_1 y_2 |\mathbf{k}_\perp \times \mathbf{q}_\perp| + (x_2 y_2 + x_1 y_1)|\mathbf{k}_\perp \times \mathbf{l}_\perp| \right], \\
F_{A1} &= \frac{-2}{x_1 x_2 y_1 y_2} \left[\mathbf{k}_\perp \cdot \mathbf{l}_\perp + x_2(\mathbf{l}_\perp \cdot \mathbf{q}_\perp) + (x_1 y_1 + x_2 y_2)m^2 \right] + \frac{2}{(x_1 - y_1)}[D_2 + D_4] = F_A + \frac{2}{(x_1 - y_1)}[D_2 + D_4], \\
F_{A2} &= F_A + \frac{2}{(x_1 - y_1)}[D_2 + D_4], \quad F_{A3} = F_A + \frac{2}{(x_1 - y_1)}[D_2 - D_4], \\
G_A &= \frac{2}{x_1 x_2 y_1 y_2} \left[2x_1 y_1 y_2 |\mathbf{k}_\perp \times \mathbf{q}_\perp| - x_2 |\mathbf{l}_\perp \times \mathbf{q}_\perp| + (1 - 2x_1 y_1) |\mathbf{k}_\perp \times \mathbf{l}_\perp| \right], \tag{A1}
\end{aligned}$$

for the diagrams A_i and

$$\begin{aligned}
P_{B1} &= \frac{-2}{x_1 x_2 y_1 y_2} \left[x_1 x_2 y_2^2 \mathbf{q}_\perp^2 + x_1 x_2 \mathbf{l}_\perp^2 + y_1 y_2 \mathbf{k}_\perp^2 - y_2(x_1 y_1 + x_2 y_2)(\mathbf{k}_\perp \cdot \mathbf{q}_\perp) \right. \\
&\quad \left. - 2x_1 x_2 y_2(\mathbf{l}_\perp \cdot \mathbf{q}_\perp) + (x_1 y_1 + x_2 y_2)(m^2 + \mathbf{k}_\perp \cdot \mathbf{l}_\perp) \right] + \frac{2}{(y_2 - x_2)}[D_9 + D_7] = P_B + \frac{2}{(y_2 - x_2)}[D_9 + D_7], \\
P_{B2} &= P_B + \frac{2}{(x_2 - y_2)}[D_9 + D_7], \quad P_{B3} = P_B + \frac{2}{(y_2 - x_2)}[D_9 - D_7], \\
Q_B &= \frac{2}{x_1 x_2 y_1 y_2} (x_1 y_1 - x_2 y_2)(|\mathbf{l}_\perp \times \mathbf{k}_\perp| - y_2 |\mathbf{q}_\perp \times \mathbf{k}_\perp|), \\
F_{B1} &= \frac{-2}{x_1 x_2 y_1 y_2} \left[\mathbf{k}_\perp \cdot \mathbf{l}_\perp - y_2(\mathbf{k}_\perp \cdot \mathbf{q}_\perp) + (x_1 y_1 + x_2 y_2)m^2 \right] + \frac{2}{(y_2 - x_2)}[D_9 + D_7] = F_B + \frac{2}{(y_2 - x_2)}[D_9 + D_7], \\
F_{B2} &= F_B + \frac{2}{(x_2 - y_2)}[D_9 + D_7], \quad F_{B3} = F_B + \frac{2}{(y_2 - x_2)}[D_9 - D_7], \\
G_B &= \frac{2}{x_1 x_2 y_1 y_2} (y_2 |\mathbf{q}_\perp \times \mathbf{k}_\perp| - |\mathbf{l}_\perp \times \mathbf{k}_\perp|), \tag{A2}
\end{aligned}$$

for the diagrams B_i , respectively.

As an illustration, we show how to obtain the hard scattering amplitudes $T_A = \sum_{i=1}^3 T_{A_i}$ (sixth column in Table IV) and $T_B = \sum_{i=1}^3 T_{B_i}$ (sixth column in Table V)

as well as the total amplitude $T_H = T_A + T_B$ for the $(\uparrow\downarrow \rightarrow \uparrow\downarrow)$ contribution. Using the identities Eqs. (38) and (39) in Sec.III, we obtain

$$\begin{aligned}
\left[\sum_i T_{A_i}^{(\uparrow\downarrow \rightarrow \uparrow\downarrow)} \right]_{\Delta=0} &= -8\pi\alpha_s C_F \left[\frac{\theta(y_2 - x_2)(P_{A1} + iQ_A)}{(y_2 - x_2)\mathcal{D}_1\mathcal{D}_2} + \frac{\theta(x_2 - y_2)(P_{A2} + iQ_A)}{(x_2 - y_2)\mathcal{D}_3\mathcal{D}_4} + \frac{\theta(x_2 - y_2)(P_{A3} + iQ_A)}{(x_2 - y_2)\mathcal{D}_5\mathcal{D}_6} \right] \\
&= -8\pi\alpha_s C_F (P_A + iQ_A) \left[\frac{\theta(y_2 - x_2)}{(y_2 - x_2)\mathcal{D}_1\mathcal{D}_2} + \frac{\theta(x_2 - y_2)}{(x_2 - y_2)} \left(\frac{1}{\mathcal{D}_3\mathcal{D}_4} + \frac{1}{\mathcal{D}_5\mathcal{D}_6} \right) \right] \\
&\quad - 16\pi\alpha_s C_F \left[\frac{\theta(y_2 - x_2)}{(y_2 - x_2)^2} \frac{\mathcal{D}_2 + \mathcal{D}_4}{\mathcal{D}_1\mathcal{D}_2} + \frac{\theta(x_2 - y_2)}{(x_2 - y_2)^2} \left(\frac{\mathcal{D}_2 + \mathcal{D}_4}{\mathcal{D}_3\mathcal{D}_4} + \frac{\mathcal{D}_2 - \mathcal{D}_4}{\mathcal{D}_5\mathcal{D}_6} \right) \right] \\
&= -8\pi\alpha_s C_F (P_A + iQ_A) \left[\frac{1}{(y_2 - x_2)\mathcal{D}_1\mathcal{D}_2} \right] - 8\pi\alpha_s C_F \left[\frac{2}{(y_2 - x_2)^2 \mathcal{D}_2} \right], \tag{A3}
\end{aligned}$$

and

$$\begin{aligned}
\left[\sum_i T_{B_i}^{(\uparrow\downarrow \rightarrow \uparrow\downarrow)} \right]_{\Delta=0} &= -8\pi\alpha_s C_F \left[\frac{\theta(y_2 - x_2)(P_{B_1} + iQ_B)}{(y_2 - x_2)\mathcal{D}_7\mathcal{D}_8} + \frac{\theta(y_2 - x_2)(P_{B_3} + iQ_B)}{(y_2 - x_2)\mathcal{D}_{11}\mathcal{D}_{12}} + \frac{\theta(x_2 - y_2)(P_{B_2} + iQ_B)}{(x_2 - y_2)\mathcal{D}_9\mathcal{D}_{10}} \right] \\
&= -8\pi\alpha_s C_F (P_B + iQ_B) \left[\frac{\theta(y_2 - x_2)}{(y_2 - x_2)} \left(\frac{1}{\mathcal{D}_7\mathcal{D}_8} + \frac{1}{\mathcal{D}_{11}\mathcal{D}_{12}} \right) + \frac{\theta(x_2 - y_2)}{(x_2 - y_2)\mathcal{D}_9\mathcal{D}_{10}} \right] \\
&\quad - 16\pi\alpha_s C_F \left[\frac{\theta(y_2 - x_2)}{(y_2 - x_2)^2} \left(\frac{\mathcal{D}_9 + \mathcal{D}_7}{\mathcal{D}_7\mathcal{D}_8} + \frac{\mathcal{D}_9 - \mathcal{D}_7}{\mathcal{D}_{11}\mathcal{D}_{12}} \right) + \frac{\theta(x_2 - y_2)}{(x_2 - y_2)^2} \frac{\mathcal{D}_9 + \mathcal{D}_7}{\mathcal{D}_9\mathcal{D}_{10}} \right] \\
&= -8\pi\alpha_s C_F (P_B + iQ_B) \left[\frac{1}{(y_2 - x_2)\mathcal{D}_2\mathcal{D}_8} \right] - 8\pi\alpha_s C_F \left[\frac{2}{(y_2 - x_2)^2\mathcal{D}_5} \right], \tag{A4}
\end{aligned}$$

where the first terms in Eqs. (A3) and (A4) proportional to $1/(y_2 - x_2)$ and the second terms proportional to $1/(y_2 - x_2)^2$ are related with the Feynman gauge and the LF gauge parts, respectively. By adding all six LF time-ordered diagrams, we obtain

$$\begin{aligned}
T_H^{(\uparrow\downarrow \rightarrow \uparrow\downarrow)} &= \sum_i \left[T_{A_i}^{(\uparrow\downarrow \rightarrow \uparrow\downarrow)} + T_{B_i}^{(\uparrow\downarrow \rightarrow \uparrow\downarrow)} \right]_{\Delta=0} \\
&= -\frac{8\pi\alpha_s C_F}{(y_2 - x_2)} \left[\frac{(P_A + iQ)}{\mathcal{D}_1\mathcal{D}_2} + \frac{(P_B + iQ_B)}{\mathcal{D}_2\mathcal{D}_8} \right], \tag{A5}
\end{aligned}$$

i.e. the singular LF gauge parts cancel each other and only finite Feynman gauge parts contribute to the amplitude. Similarly, we obtain other helicity contributions to the hard scattering amplitude as shown in Tables IV and V.

APPENDIX B: HARD SCATTERING AMPLITUDE COMBINED WITH RELATIVISTIC SPIN-ORBIT WAVE FUNCTION

In this appendix B, we list the leading and subleading helicity contributions to the hard scattering amplitude combined with the relativistic spin-orbit wave function, where the subleading helicity contributions show up as next-to-leading order in transverse momenta. That is, the subleading helicity contributions vanish at leading twist.

We first consider the relativistic spin-orbit wave functions for pseudoscalar and vector(with transverse polarization $\epsilon = +1$) mesons given by Eqs. (4) and (6), respectively. Besides the leading helicity(in transverse momenta) contributions coming from two $\Delta H = 1$ contributions(i.e. $\uparrow\downarrow \rightarrow \uparrow\uparrow$ and $\downarrow\uparrow \rightarrow \uparrow\uparrow$), the subleading helicity contributions are as follows.

(1) $\Delta H = 0$ contributions:

$$\begin{aligned}
\mathcal{R}_{\uparrow\downarrow}^{11\uparrow}\mathcal{R}_{\uparrow\downarrow}^{00} &= \frac{m\sqrt{2}}{C_x C_y} \left[\frac{y_1 M_{0y} + m}{M_{0y} + 2m} \right] l^L = -\mathcal{R}_{\uparrow\downarrow}^{11\uparrow}\mathcal{R}_{\uparrow\downarrow}^{00}, \\
\mathcal{R}_{\downarrow\uparrow}^{11\uparrow}\mathcal{R}_{\downarrow\uparrow}^{00} &= \frac{m\sqrt{2}}{C_x C_y} \left[\frac{y_2 M_{0y} + m}{M_{0y} + 2m} \right] l^L = -\mathcal{R}_{\downarrow\uparrow}^{11\uparrow}\mathcal{R}_{\downarrow\uparrow}^{00}, \\
\mathcal{R}_{\uparrow\uparrow}^{11\uparrow}\mathcal{R}_{\uparrow\uparrow}^{00} &= -\frac{\sqrt{2}}{C_x C_y} \left[m + \frac{\mathbf{l}_\perp^2}{M_{0y} + 2m} \right] k^L \\
\mathcal{R}_{\downarrow\downarrow}^{11\uparrow}\mathcal{R}_{\downarrow\downarrow}^{00} &= \frac{\sqrt{2}}{C_x C_y} \left[\frac{1}{M_{0y} + 2m} \right] k^R (l^L)^2. \tag{B1}
\end{aligned}$$

(2) $\Delta H = 1$ contributions:

$$\begin{aligned}
\mathcal{R}_{\downarrow\downarrow}^{11\uparrow}\mathcal{R}_{\downarrow\downarrow}^{00} &= \frac{m\sqrt{2}}{C_x C_y} \left[\frac{1}{M_{0y} + 2m} \right] (l^L)^2 = -\mathcal{R}_{\downarrow\downarrow}^{11\uparrow}\mathcal{R}_{\downarrow\downarrow}^{00}, \\
\mathcal{R}_{\uparrow\downarrow}^{11\uparrow}\mathcal{R}_{\uparrow\downarrow}^{00} &= -\frac{\sqrt{2}}{C_x C_y} \left[\frac{y_1 M_{0y} + m}{M_{0y} + 2m} \right] l^L k^L, \\
\mathcal{R}_{\uparrow\downarrow}^{11\uparrow}\mathcal{R}_{\uparrow\downarrow}^{00} &= -\frac{\sqrt{2}}{C_x C_y} \left[\frac{y_1 M_{0y} + m}{M_{0y} + 2m} \right] l^L k^R, \\
\mathcal{R}_{\downarrow\uparrow}^{11\uparrow}\mathcal{R}_{\downarrow\uparrow}^{00} &= \frac{\sqrt{2}}{C_x C_y} \left[\frac{y_2 M_{0y} + m}{M_{0y} + 2m} \right] l^L k^L, \\
\mathcal{R}_{\downarrow\uparrow}^{11\uparrow}\mathcal{R}_{\downarrow\uparrow}^{00} &= \frac{\sqrt{2}}{C_x C_y} \left[\frac{y_2 M_{0y} + m}{M_{0y} + 2m} \right] l^L k^R. \tag{B2}
\end{aligned}$$

where $C_x = \sqrt{2x_1 x_2} M_{0x}$ and $C_y = \sqrt{2y_1 y_2} M_{0y}$. Since the hard scattering amplitudes vanish for $\Delta H = 2$ cases, we do not consider them here.

Next, we obtain the hard scattering amplitude combined with the spin-orbit wave function.

(1) $\Delta H = 0$ contributions:

$$\begin{aligned}
\mathcal{T}_H^R(\uparrow\downarrow \rightarrow \uparrow\downarrow) &= \frac{\sqrt{2}}{q^L} \mathcal{R}_{\uparrow\downarrow}^{11\uparrow} T_H^{(\uparrow\downarrow \rightarrow \uparrow\downarrow)} \mathcal{R}_{\uparrow\downarrow}^{00} \\
&= \frac{16\pi\alpha_s C_F m}{(y_2 - x_2) C_x C_y q^2} \left[\frac{y_1 M_{0y} + m}{M_{0y} + 2m} \right] \\
&\quad \times (l^L q^R) \left[\frac{P_A + iQ_A}{\mathcal{D}_1\mathcal{D}_2} + \frac{P_B + iQ_B}{\mathcal{D}_2\mathcal{D}_8} \right], \tag{B3}
\end{aligned}$$

$$\begin{aligned}
\mathcal{T}_H^R(\downarrow\uparrow\rightarrow\downarrow\uparrow) &= \frac{\sqrt{2}}{q^L} \mathcal{R}_{\downarrow\uparrow}^{11\dagger} T_H^{(\downarrow\uparrow\rightarrow\downarrow\uparrow)} \mathcal{R}_{\downarrow\uparrow}^{00} \\
&= \frac{16\pi\alpha_s C_F m}{(y_2 - x_2) C_x C_y q^2} \left[\frac{y_2 M_{0y} + m}{M_{0y} + 2m} \right] \\
&\quad \times (l^L q^R) \left[\frac{P_A - iQ_A}{\mathcal{D}_1 \mathcal{D}_2} + \frac{P_B - iQ_B}{\mathcal{D}_2 \mathcal{D}_8} \right], \quad (\text{B4})
\end{aligned}$$

$$\begin{aligned}
\mathcal{T}_H^R(\uparrow\uparrow\rightarrow\uparrow\uparrow) &= \frac{\sqrt{2}}{q^L} \mathcal{R}_{\uparrow\uparrow}^{11\dagger} T_H^{(\uparrow\uparrow\rightarrow\uparrow\uparrow)} \mathcal{R}_{\uparrow\uparrow}^{00} \\
&= \frac{-16\pi\alpha_s C_F}{(y_2 - x_2) C_x C_y q^2} \left[m + \frac{\mathbf{l}_\perp^2}{M_{0y} + 2m} \right] \\
&\quad \times (k^L q^R) \left[\frac{F_A + iG_A}{\mathcal{D}_1 \mathcal{D}_2} + \frac{F_B + iG_B}{\mathcal{D}_2 \mathcal{D}_8} \right], \quad (\text{B5})
\end{aligned}$$

$$\begin{aligned}
\mathcal{T}_H^R(\downarrow\downarrow\rightarrow\downarrow\downarrow) &= \frac{\sqrt{2}}{q^L} \mathcal{R}_{\downarrow\downarrow}^{11\dagger} T_H^{(\downarrow\downarrow\rightarrow\downarrow\downarrow)} \mathcal{R}_{\downarrow\downarrow}^{00} \\
&= \frac{16\pi\alpha_s C_F}{(y_2 - x_2) C_x C_y q^2} \left[\frac{1}{M_{0y} + 2m} \right] \\
&\quad \times (k^R l^L l^L q^R) \left[\frac{F_A - iG_A}{\mathcal{D}_1 \mathcal{D}_2} + \frac{F_B - iG_B}{\mathcal{D}_2 \mathcal{D}_8} \right], \quad (\text{B6})
\end{aligned}$$

$$\begin{aligned}
\mathcal{T}_H^R(\uparrow\downarrow\rightarrow\downarrow\uparrow) &= \frac{\sqrt{2}}{q^L} \mathcal{R}_{\downarrow\uparrow}^{11\dagger} T_H^{(\uparrow\downarrow\rightarrow\downarrow\uparrow)} \mathcal{R}_{\downarrow\uparrow}^{00} \\
&= \frac{32\pi\alpha_s C_F m^3 (y_1 - x_1)}{x_1 x_2 y_1 y_2 C_x C_y q^2} \left[\frac{y_2 M_{0y} + m}{M_{0y} + 2m} \right] \\
&\quad \times (l^L q^R) \left[\frac{1}{\mathcal{D}_1 \mathcal{D}_2} + \frac{1}{\mathcal{D}_2 \mathcal{D}_8} \right], \quad (\text{B7})
\end{aligned}$$

$$\begin{aligned}
\mathcal{T}_H^R(\downarrow\uparrow\rightarrow\uparrow\downarrow) &= \frac{\sqrt{2}}{q^L} \mathcal{R}_{\uparrow\downarrow}^{11\dagger} T_H^{(\downarrow\uparrow\rightarrow\uparrow\downarrow)} \mathcal{R}_{\uparrow\downarrow}^{00} \\
&= \frac{32\pi\alpha_s C_F m^3 (y_1 - x_1)}{x_1 x_2 y_1 y_2 C_x C_y q^2} \left[\frac{y_1 M_{0y} + m}{M_{0y} + 2m} \right] \\
&\quad \times (l^L q^R) \left[\frac{1}{\mathcal{D}_1 \mathcal{D}_2} + \frac{1}{\mathcal{D}_2 \mathcal{D}_8} \right]. \quad (\text{B8})
\end{aligned}$$

(2) $\Delta H = 1$ contributions:

$$\begin{aligned}
\mathcal{T}_H^R(\uparrow\downarrow\rightarrow\downarrow\downarrow) &= \frac{\sqrt{2}}{q^L} \mathcal{R}_{\downarrow\downarrow}^{11\dagger} T_H^{(\uparrow\downarrow\rightarrow\downarrow\downarrow)} \mathcal{R}_{\downarrow\downarrow}^{00} \\
&= \frac{-32\pi\alpha_s C_F m^2}{x_1 y_1 y_2 (y_2 - x_2) C_x C_y q^2} \left[\frac{1}{M_{0y} + 2m} \right] \\
&\quad \times (l^L q^R) \left[\frac{x_2 \mathbf{l}_\perp^2 - y_2 l^L k^R - x_2 y_2 l^L q^R}{\mathcal{D}_1 \mathcal{D}_2} \right. \\
&\quad \left. + \frac{x_2 \mathbf{l}_\perp^2 - y_2 l^L k^R - x_2 y_2 l^L q^R}{\mathcal{D}_2 \mathcal{D}_8} \right], \quad (\text{B9})
\end{aligned}$$

$$\begin{aligned}
\mathcal{T}_H^R(\downarrow\uparrow\rightarrow\downarrow\downarrow) &= \frac{\sqrt{2}}{q^L} \mathcal{R}_{\downarrow\downarrow}^{11\dagger} T_H^{(\downarrow\uparrow\rightarrow\downarrow\downarrow)} \mathcal{R}_{\downarrow\downarrow}^{00} \\
&= \frac{-32\pi\alpha_s C_F m^2}{x_2 y_1 y_2 (y_2 - x_2) C_x C_y q^2} \left[\frac{1}{M_{0y} + 2m} \right] \\
&\quad \times (l^L q^R) \left[\frac{x_1 \mathbf{l}_\perp^2 - y_1 l^L k^R - x_2 y_1 l^L q^R}{\mathcal{D}_1 \mathcal{D}_2} \right. \\
&\quad \left. + \frac{x_1 \mathbf{l}_\perp^2 - y_1 l^L k^R - x_2 y_2 l^L q^R}{\mathcal{D}_2 \mathcal{D}_8} \right], \quad (\text{B10})
\end{aligned}$$

$$\begin{aligned}
\mathcal{T}_H^R(\uparrow\uparrow\rightarrow\uparrow\downarrow) &= \frac{\sqrt{2}}{q^L} \mathcal{R}_{\uparrow\downarrow}^{11\dagger} T_H^{(\uparrow\uparrow\rightarrow\uparrow\downarrow)} \mathcal{R}_{\uparrow\downarrow}^{00} \\
&= \frac{32\pi\alpha_s C_F m}{x_1 x_2 y_2 (y_2 - x_2) C_x C_y q^2} \left[\frac{y_1 M_{0y} + m}{M_{0y} + 2m} \right] \\
&\quad \times (l^L q^R) \left[\frac{x_1 k^L l^R - y_1 \mathbf{k}_\perp^2 - x_2 y_1 k^L q^R}{\mathcal{D}_1 \mathcal{D}_2} \right. \\
&\quad \left. + \frac{x_1 k^L l^R - y_1 \mathbf{k}_\perp^2 - x_1 y_2 k^L q^R}{\mathcal{D}_2 \mathcal{D}_8} \right], \quad (\text{B11})
\end{aligned}$$

$$\begin{aligned}
\mathcal{T}_H^R(\downarrow\downarrow\rightarrow\uparrow\downarrow) &= \frac{\sqrt{2}}{q^L} \mathcal{R}_{\uparrow\downarrow}^{11\dagger} T_H^{(\downarrow\downarrow\rightarrow\uparrow\downarrow)} \mathcal{R}_{\uparrow\downarrow}^{00} \\
&= \frac{32\pi\alpha_s C_F m}{x_1 x_2 y_1 (y_2 - x_2) C_x C_y q^2} \left[\frac{y_1 M_{0y} + m}{M_{0y} + 2m} \right] \\
&\quad \times (l^L q^R) \left[\frac{x_2 l^L k^R - y_2 \mathbf{k}_\perp^2 - x_2 y_2 q^L k^R}{\mathcal{D}_1 \mathcal{D}_2} \right. \\
&\quad \left. + \frac{x_2 l^L k^R - y_2 \mathbf{k}_\perp^2 - x_2 y_2 q^L k^R}{\mathcal{D}_2 \mathcal{D}_8} \right], \quad (\text{B12})
\end{aligned}$$

$$\begin{aligned}
\mathcal{T}_H^R(\uparrow\uparrow\rightarrow\uparrow\downarrow) &= \frac{\sqrt{2}}{q^L} \mathcal{R}_{\uparrow\downarrow}^{11\dagger} T_H^{(\uparrow\uparrow\rightarrow\uparrow\downarrow)} \mathcal{R}_{\uparrow\downarrow}^{00} \\
&= \frac{32\pi\alpha_s C_F m}{x_1 x_2 y_1 (y_2 - x_2) C_x C_y q^2} \left[\frac{y_2 M_{0y} + m}{M_{0y} + 2m} \right] \\
&\quad \times (l^L q^R) \left[\frac{x_2 k^L l^R - y_2 \mathbf{k}_\perp^2 - x_2 y_2 k^L q^R}{\mathcal{D}_1 \mathcal{D}_2} \right. \\
&\quad \left. + \frac{x_2 k^L l^R - y_2 \mathbf{k}_\perp^2 - x_2 y_2 k^L q^R}{\mathcal{D}_2 \mathcal{D}_8} \right], \quad (\text{B13})
\end{aligned}$$

$$\begin{aligned}
\mathcal{T}_H^R(\downarrow\downarrow\rightarrow\uparrow\uparrow) &= \frac{\sqrt{2}}{q^L} \mathcal{R}_{\uparrow\uparrow}^{11\dagger} T_H^{(\downarrow\downarrow\rightarrow\uparrow\uparrow)} \mathcal{R}_{\uparrow\uparrow}^{00} \\
&= \frac{32\pi\alpha_s C_F m}{x_1 x_2 y_2 (y_2 - x_2) C_x C_y q^2} \left[\frac{y_2 M_{0y} + m}{M_{0y} + 2m} \right] \\
&\quad \times (l^L q^R) \left[\frac{x_1 l^L k^R - y_1 \mathbf{k}_\perp^2 - x_2 y_1 q^L k^R}{\mathcal{D}_1 \mathcal{D}_2} \right. \\
&\quad \left. + \frac{x_1 l^L k^R - y_1 \mathbf{k}_\perp^2 - x_1 y_2 q^L k^R}{\mathcal{D}_2 \mathcal{D}_8} \right]. \quad (\text{B14})
\end{aligned}$$

-
- [1] S.J. Brodsky and C.-R. Ji, Phys. Rev. Lett. **55**, 2257 (1985).
 - [2] E. Braaten and J. Lee, Phys. Rev. D **67**, 054007 (2003); **72**, 099901(E) (2005).
 - [3] K.-Y. Liu, Z.-G. He, and K.-T. Chao, Phys. Lett. B **557**, 45 (2003).
 - [4] K. Hagiwara, E. Kou, and C.-F. Qiao, Phys. Lett. B **570**, 39 (2003).
 - [5] V.V. Kiselev, Int. J. Mod. Phys. A **10**, 465 (1995).
 - [6] G.T. Bodwin, E. Braaten, and G.P. Lepage, Phys. Rev. D **51**, 1125 (1995); **55**, 5853(E) (1997).
 - [7] K. Abe *et al.* (Belle Collaboration), Phys. Rev. Lett. **89**, 142001 (2002); Phys. Rev. D **70**, 071102 (2004).
 - [8] B. Aubert *et al.* (Babar Collaboration), Phys. Rev. D **72**, 031101 (2005).
 - [9] A.E. Bondar and V.L. Chernyak, Phys. Lett. B **612**, 215 (2005).
 - [10] J.P. Ma and Z.G. Si, Phys. Rev. D **70**, 074007 (2004).
 - [11] V.V. Braguta, A.K. Likhoded, and A.V. Luchinsky, Phys. Rev. D **72**, 074019 (2005).
 - [12] T. Huang and F. Zuo, arXiv:hep-ph/0702147v2.
 - [13] C.-R. Ji and A. Pang, Phys. Rev. D **55**, 1253 (1997).
 - [14] H.-M. Choi and C.-R. Ji, Phys. Rev. D **73**, 114020 (2006).
 - [15] H.-M. Choi and C.-R. Ji, Phys. Rev. D **59**, 074015 (1999).
 - [16] H.-M. Choi and C.-R. Ji, Phys. Lett. B **460**, 461 (1999).
 - [17] D. Ebert and A.P. Martynenko, Phys. Rev. D **74**, 054008 (2006).
 - [18] Y.-J. Zhang, Y.-J. Gao, and K.T. Chao, Phys. Rev. Lett. **96**, 092001 (2006).
 - [19] G. P. Lepage and S. J. Brodsky, Phys. Rev. D **22**, 2157 (1980); S.J. Brodsky, T. Huang, and G.P. Lepage, in *Particles and Fields-2*, Proceedings of the Banff Summer Institute, Banff, Alberta, 1981, edited by A.Z. Capri and A.N. Kamal (Plenum, New York, 1983), p. 143.
 - [20] H.-M. Choi and C.-R. Ji, Phys. Rev. D **75**, 034019 (2007).
 - [21] H.-M. Choi and C.-R. Ji, Phys. Rev. D **72**, 013004 (2005).
 - [22] C.-R. Ji, A. Pang, and A. Szczepaniak, Phys. Rev. D **52**, 4038 (1995).
 - [23] T. Huang, X.-G. Wu, and X.-H. Wu, Phys. Rev. D **70**, 053007 (2004).
 - [24] S. Godfrey and N. Isgur, Phys. Rev. D **32**, 189 (1985); S. Godfrey, Phys. Rev. D **33**, 1391 (1986).
 - [25] D. Scora and N. Isgur, Phys. Rev. D **52**, 2783 (1995).
 - [26] E. Eichten, K. Gottfried, T. Kinoshita, K.D. Lane and T.M. Yan, Phys. Rev. D **17**, 3090 (1978) [Erratum-ibid. D **21**, 313 (1980)].
 - [27] G.T. Bodwin, D. Kang and J. Lee, Phys. Rev. D **74**, 114028 (2006).
 - [28] G.S. Bali, Phys. Rept. **343**, 1 (2001).
 - [29] K.W. Edwards *et al.*, CLEO Collaboration, Phys. Rev. Lett. **86**, 30 (2001).
 - [30] W.-M. Yao *et al.* (Particle Data Group), J. Phys. G **33**, 1 (2006).
 - [31] V.V. Braguta, A.K. Likhoded, and A.V. Luchinsky, Phys. Lett. B **646**, 80 (2007).
 - [32] V.V. Braguta, Phys. Rev. D **75**, 094016 (2007).
 - [33] W. Buchmuller and S.H.H. Tye, Phys. Rev. D **24**, 132 (1981).
 - [34] G.T. Bodwin, D. Kang and J. Lee, Phys. Rev. D **74**, 014014 (2006).
 - [35] X.D. Ji, J.P. Ma and F. Yuan, Phys. Rev. Lett. **90**, 241601 (2003).
 - [36] S.J. Brodsky and G.R. Farrar, Phys. Rev. Lett. **31**, 1153 (1973); Phys. Rev. D **11**, 1309 (1975).
 - [37] V.A. Matveev, R.M. Muradian and A.N. Tavkhelidze, Nuovo Cim. Lett. **7**, 719 (1973).
 - [38] C.E. Carlson and C.-R. Ji, Phys. Rev. D **67**, 116002 (2003).
 - [39] B.L.G. Bakker and C.-R. Ji, Phys. Rev. D **65**, 073002 (2002).
 - [40] Through the private communication with Jungil Lee and Stan Brodsky, we have indeed confirmed the agreement between the NRQCD result and the peaking approximation result of PQCD.